THE UNIVERSITY OF MANITOBA

TRANSVERSE CONFINEMENT OF STEEL FREE DECK SLABS BY PRESTRESSED CONCRETE STRAPS

By

VAIBHAV BANTHIA

A Thesis Submitted to the
Faculty of Graduate Studies in partial fulfilment
of the requirements for the
Degree of Master of Science

DEPARTMENT OF CIVIL ENGINEERING
WINNIPEG, MANITOBA
March 2003

THE UNIVERSITY OF MANITOBA

FACULTY OF GRADUATE STUDIES

*****

COPYRIGHT PERMISSION PAGE

TRANSVERSE CONFINEMENT OF STEEL FREE DECK SLABS BY PRESTRESSED CONCRETE STRAPS

BY

VAIBHAV BANTHIA

A Thesis/Practicum submitted to the Faculty of Graduate Studies of The University of Manitoba in partial fulfillment of the requirements of the degree of

Master of Science

ACKNOWLEDGEMENTS

I take this opportunity to express my sincere gratitude to both Dr. Aftab. A. Mufti and Dr. Baidar Bakht for their professional encouragement and technical guidance. Being the pioneers of steel free deck slabs, their advice was always propitious and helpful. Thanks are due to Dr. Dagmar Svecova for providing guidance for the design and construction of the prestressed concrete straps.

I would like to thank Dr. Mufti again, for providing financial support through grants from Canadian Centers of Excellence on Intelligent Sensing for Innovative Structures, ISIS Canada.

The laboratory assistance of Mr. Moray McVey, Mr. Grant Whiteside and Mr. Scott Sparrow is thankfully acknowledged. Also recognised is the valuable administrative and clerical assistance provided by ISIS Canada, Manitoba. My special thanks to the fellow graduate students for their help and support during my Master's Program.

I would like to thank all my family members, especially my parents for their constant encouragement and blessings and last but not the least, to my wife Shweta for being my pillar of strength.

ABSTRACT

Research conducted over the past ten or so years has shown that concrete deck slabs supported on parallel beams derive their high load carrying capacities from both transverse and longitudinal confinement. The transverse confinement, provided by external straps, serve the function of restraining the lateral movement of the top of the girders, which is induced by the arching action in the slab. It is now well established that the axial stiffness – rather than the strength – of the transverse confining system governs the load carrying capacity of the slab. The Canadian Highway Bridge Design Code (CHBDC, 2000) specifies an equation for the cross-sectional area, A, of straps in fibre reinforced concrete (FRC) steel free deck slabs. According to this equation, A is inversely proportional to the modulus of elasticity of the material of the strap.

Realising that the substantial modulus of elasticity of concrete in a component in tension can be mobilised prior to cracking, it was decided to study experimentally the axial stiffness of concrete straps of rectangular cross-section. The experimental study included the testing of prestressed concrete straps in tension with a cross-section of 150×100 mm. Each strap was pretensioned with two 15 mm diameter bars of glass fibre reinforced polymer (GFRP).

The tests have confirmed that within the expected range of tensile forces, the 150×100 mm prestressed concrete straps behave in a linear elastic manner, with their initial stiffness being about two times larger than that of 50×25 mm steel straps.

Based on this outcome, it was decided to use prestressed concrete straps as transverse confinement in deck slabs without reinforcement. A fatigue study was done on the full scale partial model of the said deck slab, subjecting it to 500,000 cycles of a 208 kN load, which simulated the lifetime's damage induced by vehicular traffic on a typical bridge deck.

TABLE OF CONTENTS

LIST OF TABLES

LIST OF FIGURES

Chapter 6

Chapter 7

Chapter 8

LIST OF SYMBOLS AND ABBREVIATIONS

Acronyms

AFRP	Aramid Fibre Reinforced Polymer
ASTM	American Society for Testing and Materials
CFRP	Carbon Fibre Reinforced Polymer
CHBDC	Canadian Highway Bridge Design Code
CL-625	Canadian Loading for the design of national highway network
CSA	Canadian Standards Association
FRC	Fibre Reinforced Concrete
FRP	Fibre Reinforced Polymer
GFRP	Glass Fibre Reinforced Polymer
LVDT	Linear Variable Displacement Transducer
OHBDC	Ontario Highway Bridge Design Code

Symbols

A	Area of cross-section of strap
A_c	Cross sectional area of concrete strap
A_p, A_{frp}	Cross sectional area of prestressing tendon
A_s	Cross sectional area of reinforcing steel
A_{sc}	Cross sectional area of stud
d	Diameter of concrete cylinder
E	Modulus of elasticity of the strap material
E_c	Modulus of elasticity of concrete
E_p	Modulus of elasticity of prestressing tendon
F	Applied load on the strap
F_u	Tensile strength of steel stud
f'_c	Compressive strength of concrete
f_c	Stress in concrete
f_{cr}	Direct cracking strength

f_{frp}	Stress in FRP tendon
f_r	Modulus of rupture
f_s	Stress in steel reinforcing bars
f_{sp}	Concrete splitting strength
f'_t	Tensile strength of concrete
h_{slab},t	Thickness of deck slab
k_p	Stiffness of the prestressing tendon
k_c	Stiffness of concrete
L_c	Length of concrete strap
L_p	Length of the prestressing tendon
l	Length of the concrete cylinder
N	Axial load
n	Number of test specimen
q_r	Factored shear resistance of a headed shear stud
R_k	Stiffness ratio
S_l	The spacing of straps
V_{FRP}	Coefficient of variation of tensile strength
W	Concrete unit weight
Δ	Axial deformation
γ_c	Mass density of concrete
ϕ_{sc}	Resistance factor
ε	Strain in strap
ε_c	Strain in concrete
ε_s	Strain in reinforcing steel
ε_p	Strain in prestressing tendon
ε'_t	Strain corresponding to the maximum stress, f'_t
β	Parameter depending upon the shape of the stress strain diagram
σ	Stress in strap

Chapter 1

INTRODUCTION

1.1. Background

Many types of highway bridges are in use today, ranging from suspension structures to short slab bridges. Girder bridges with concrete deck slabs are the most common types of highway bridges in North America. The deck slabs of these bridges in particularly cold climate, like that of Canada, experience most significant deterioration. This deterioration is caused by the corrosion of steel bars in the concrete, which is saturated with chlorides from deicing salts. To remove this cause of deterioration, i.e. steel reinforcement, the concept of steel free deck slabs has evolved (Mufti, et al. 1991).

It has been successfully demonstrated that the removal of all internal reinforcing steel from the deck slab of concrete slab on girder bridges is possible. The internal steel reinforcement is not replaced with another synthetic or non-ferrous reinforcement; but rather the whole bridge deck system is modified with a system of external steel straps. Such a system is now being referred to as steel-free bridge deck system. Under a concentrated load, the presence of the internal arching system causes the slab to fail in punching shear rather than in flexure (Mufti, et al. 1991).

Previous experimental testing has demonstrated the feasibility of the concept and the substantial ultimate load capacity of the system by means of tests conducted, initially on small-scale specimens and then after being proven satisfactory, on full size concrete deck slab, subjecting it to either static or pulsating loads (Mufti, et al. 1993, Bakht and Agarwal 1995, Thorburn and Mufti, 1995, Newhook and Mufti, 1996, Matsui et al. 2001). The outcome of this approach is considerable saving in the amount of reinforcement required. The reduced amount of steel has the additional benefit of enhancing the durability of concrete against the effect of steel corrosion.

The problem of corrosion of steel in concrete deck slab has, to date, been addressed in a number of ways, such as-

- Coating the steel reinforcing bars by epoxy or other protective materials
- Increasing the depth of concrete cover over the steel bars, thereby increasing the overall thickness of the slab
- Using dense concrete mixes

These costly measures have certainly improved the durability of concrete decks, however the problem of corrosion has not been eliminated completely.

Corrosion in a concrete deck slab can be eliminated entirely by replacing the steel reinforcement by rods of carbon fibres, glass fibres, or other similar new chemically inert materials. However, two factors have been so far inhibiting the common use of reinforcement bars of these new materials in bridges:

- The fibres that are comparable in their properties to steel are still too expensive for general use.
- The fibres that are relatively inexpensive have low modulus of elasticity and are unsuitable as tensile reinforcement in concrete, as their use leads to unacceptably large deformations and wide cracks.

Through tests on numerous half scale and full scale models, it has been established that fibre reinforced concrete slab with inexpensive non-ferrous fibres is

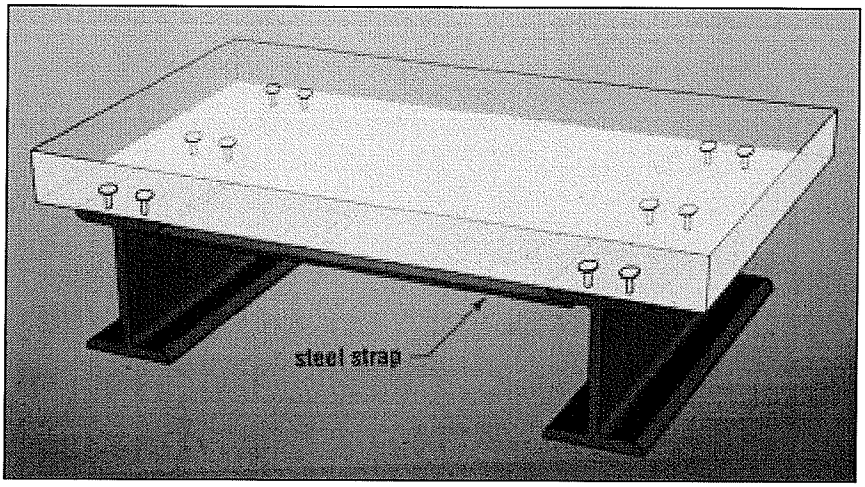

Figure 1.1
Confinement to Steel Free
Deck slab

feasible, provided that the top flanges of the steel girders are connected just below the deck by transverse steel straps and the concrete deck is joined to the girders by shear connectors. The straps and shear connectors together provide the restraint necessary for development of the internal arching system in the slab as shown in figure 1.1, whilst the randomly-mixed short synthetic low modulus fibres control the cracking due to the effects of volumetric changes like shrinkage and temperature in the concrete. Because of the use of these fibres the deck slab is referred to as *fibre reinforced concrete* (FRC) deck slab.

Concrete itself is a brittle material and cracks under low tensile stresses. Concrete also cracks due to the plastic shrinkage of concrete during curing and the thermal contraction of concrete due to environmental conditions. Plain concrete without any reinforcing steel is especially susceptible to these effects. In the steel-free deck, low modulus polypropylene fibres are added to act as a plastic crack control device and to provide some post-crack ductility to the hardened concrete slab. It should be noted that the fibres are secondary reinforcement and do not enhance the strength properties of the concrete. CHBDC, 2000 requires that the concrete of steel-free deck slabs be mixed with low modulus synthetic fibres.

1.2. History of Steel Free Bridge Deck Slabs

Many references in the literature (e.g., Hewitt and Batchelor, 1975; Beal, 1982; Fang, et al. 1986; Jackson and Cope, 1990) have confirmed that a significant arching system develops in the reinforced concrete deck slab of a slab-on-girder bridge, when it is subjected to concentrated loads. The in-plane compressive stresses generated due to this arching action cause the slab to fail in punching shear, rather than in flexure and at a much higher load.

Originally, concrete bridge deck slabs were designed as reinforced concrete with the level of reinforcement determined from assumptions of flexural failure. The slab was assumed to be a transverse bending member between a series of supporting girders. This method, called the flexural design method, led to high amounts of steel reinforcement in the slab. Continuing research revealed that the mode of failure of bridge decks was not flexure. In fact, deck slabs failed at loads that were several

times higher than predicted by flexural theory. It was determined that compressive membrane forces, sometimes referred to as internal arching forces, were being developed within the slabs and leading to a punching failure mode. These membrane forces gave the bridge deck substantial reserve capacity beyond its flexural design capacity. By taking advantage of this arching behaviour, a substantial reduction in the amount of reinforcing steel required can be realised. It was experimentally shown that for many situations 0.3% reinforcing steel in each direction, in top and bottom layer, was sufficient. In 1979, the Ontario Highway Bridge Design Code (OHBDC) was introduced which included design provisions for this empirical method. Recently published the Canadian Highway Bridge Design Code (CHBDC, 2000) has an entire chapter based on designing of Fibre Reinforced Concrete (FRC) deck slabs using the advantages of arching action.

In 1988, researchers at the Technical University of Nova Scotia began further investigations into the punching failure of concrete deck slabs. Mufti, et al. (1993) demonstrated that the entire removal of all internal steel reinforcement from the concrete slab on girder bridge decks was possible. The key to the system was the provision of adequate transverse lateral restraint so that sufficient compressive membrane forces could be developed and the deck failed in punching shear. This lateral restraint was provided by transverse steel straps, external to the deck slab, which tied the adjacent girders together. This concept has led to the world's first steel-free concrete bridge deck over Salmon River on the Trans-Canada Highway in Nova Scotia. Tests are being carried out at Dalhousie University as well as University of Manitoba to find out the effect of cyclic loading on steel-free deck slabs.

1.2.1 Steel-Free Bridge Decks in Canada

Five bridges with steel-free deck slabs have already been constructed in Canada (Bakht and Mufti, 1998). The first steel-free deck slab was cast in October 1995, on the Salmon River Bridge on the Trans Canada Highway in Nova Scotia. The 200 mm thick slab spans over steel girders at a spacing of 2.7 m. Steel straps having a 14 x 100 mm cross-section, and at a spacing of 1.2 m were welded to the top flanges of the steel girders.

The second steel-free deck slab was cast for the rehabilitation of the Kent County Road No. 10 Bridge in Chatham, Ontario. This four span bridge has steel girders at a spacing of 2.1 m. Each of the two outer spans has a 175 mm thick steel-free deck slab. The steel free deck slab is confined transversely by means of 25 x 50 mm galvanised steel straps welded to the top flanges of the girders at a spacing of 1.0 m. The Chatham Bridge was opened to traffic in November 1996.

The third steel free deck slab was the Crowchild Trail Bridge in Calgary, Alberta, which is a 185 mm thick deck slab resting on steel plate girders spaced 2 m apart. The transverse confinement is provided by 50 x 25 mm straps, which contain welded shear studs directly over the girders, typical of partially studded strap system and which will be described later. The Crowchild Trail Bridge was opened to traffic in the fall of 1997.

The fourth application of the steel free deck slab is the Waterloo Creek bridge in British Columbia. This is an integral abutment bridge with precast concrete girders having a single span of 25 m. The 190 mm thick steel free slab rests on girders at a spacing of 2.8 m. Transverse confinement of the steel free deck slab is provided by means of 50 x 25 mm studded straps at a spacing of 1.25 m. The Waterloo Creek Bridge was opened to traffic early in 1998.

Lindquist Creek Bridge is the fifth application of the steel free deck slab concept. It is a deck of precast reinforced concrete panel made composite with the girders by means of clusters of studs. Panels with a 150 mm thickness at the crown, spanning over girders at a spacing of 3.5 m are used for this bridge on a gravel forestry road in British Columbia. The transverse confinement is provided by means of 25 x 50 mm studded steel straps at a spacing of 1 m.

1.2.2 Dynamic Tests on Steel Free Deck Slabs

As static tests on steel free deck slabs provide little quantitative information about their fatigue resistance, investigation of fatigue resistance of steel free deck slab becomes a more apt choice to judge its worthiness. For instance, even if the steel free deck slab does not reach its full static strength but remain elastic under the maximum

lifetime wheel load, the deck slab would have the same fatigue resistance as that of a conventional deck slab. In this case, there should be no reason to worry about the 'full static strength of the slab,' which is never utilised anyway. Therefore, a fatigue analysis would be a better gauge to quantify the performance of a deck slab.

Following are the different types of Dynamic tests done on Steel Free Deck Slabs:

Single Moving Wheel

In this system, the moving wheel of a vehicle is represented by an actually moving single wheel, the weight and speed of which can be controlled. The test arrangement includes an anchoring frame which guides the moving wheel along a linear path. The load level on the wheel is governed by means of a vertical actuator and the movement of the wheel is controlled by a separate system of horizontal actuators with relatively long strokes. The primary advantage of such a test facility is that it replicates exactly the movement and continuous application of actual wheel loads on the surface of the test specimen. But this system has its limitations too, such as high cost, slow speed and high noise level.

Sequential Wheel Load

The shortcomings of the single moving wheel system led to the system of sequential wheel loads. In this system, the action of moving wheels is simulated by means of a number of load pads at fixed locations. The magnitude of these pads is controlled sequentially in such a way that the load is passed on from one pad to the next according to a pre-determined pattern. This passing on of the load from one wheel to another is done in such a way that during one cycle of loading the same total loads is maintained on the test specimen.

Single Pulsating Wheel Load

The load is applied through a hydraulic actuator reacting against a steel-loading frame, which is attached to the structural floor of the laboratory. The load patch simulates the dual tire footprint of a heavy highway vehicle. Though this method of fatigue testing does not replicate reality as closely as the above mentioned

procedures, but being the simplest and the most inexpensive can be regarded as a good alternative to a standard static test.

Perdikaris and Beim (1988) have demonstrated that concrete deck slabs reinforced with reduced amount of steel have higher fatigue resistance under moving loads than deck slabs with larger amount of reinforcement. This is because a fatigue crack in concrete initiates from a steel bar. Larger amounts of steel promote more severe degradation of concrete under moving loads than smaller amounts (Mufti et al. 1993).

1.3. Transverse Confining Systems for Steel Free Deck Slabs

The transverse confinement to the arching action can be provided by external means, e.g. by transverse steel straps lying outside the slab and welded to the top flanges of the girders but this system is not suitable for all situations. Bakht et al. (1997) have proposed several alternatives to welded steel straps as transverse confinement-

Confinement can be provided by steel straps with regularly spaced shear connectors. The straps have their lower faces flush with the underside of the slab and are not directly connected to the girders. Because of partial embedment in concrete, the durability of fully studded straps is expected to be the same as that of the conventional embedded reinforcement.

An alternative to the fully studded strap, the partially studded strap has shear connectors only above the girder flanges, and is not connected directly to the girders. Similar to the welded straps, this strap lies clear of the haunched slab. It can be realised that after the concrete has set around the shear connectors on both of the beams and the straps, the top flanges of the connected girders cannot move laterally without engaging the straps; therein lies the effectiveness of the system.

Another alternative is the use of Cruciform straps, which are steel straps with crossbars welded in a cruciform pattern. The straps rest on the top flanges of the girders so that the crossbars lie loosely between two adjacent rows of shear connectors. Fibre Reinforced polymer (FRP) bars, grooved strap and diaphragms can

also be used as transverse confinement. Recently another innovative idea was put into practice by using Ductal™ and corrugated sheets as permanent formwork, which acted as transverse confinement to the steel free deck slabs (Bakht et al., 2002).

Pull out tests on isolated full-scale models of the above mentioned confining systems to assess their axial stiffness have also been studied. (Bakht and Aly, 1997). The experimental models simulated the connection of the strap system with concrete girders. It was found that the connection strength for the partially studded strap system surpasses the strength required by the CHBDC by a very large margin.

1.4. Use of FRP in Structures

1.4.1 FRP as Prestressing Element

The experience to date with the structures using FRP reinforcement has served to increase the interest and willingness to use FRP reinforcement for new construction. Ultimately time will determine the feasibility of FRP reinforcement, but for now there is every indication that it will play an ever-increasing role in concrete structures.

Fibre reinforced polymer (FRP) tendons are attracting interest due to their potential for improved durability and long term cost-effectiveness for pre- and post-tensioned concrete bridge and building structures. Because FRP materials are nonmagnetic and non-corrodible, the problems of electromagnetic interference and steel corrosion can be avoided with FRP reinforcement. Additionally, FRP materials exhibit several properties, such as high tensile strength, that make them suitable for use as structural reinforcement as well as prestressing tendons (ACI committee 440, 2001). FRP tendons are usually made by the pultrusion process, where continuous high-performance fibres are continuously drawn through a liquid bath of uncured, high-strength polymer resin and through a heated oven or die in which forming and curing of the tendon takes place. As the tendon emerges from the oven or heated die, it is cooled and spooled for shipment to construction sites. Currently, all commercially available FRP tendons have proprietary ingredients that may vary over time to suit the needs of the manufacturers and customers.

Fibre reinforced polymers (FRP) have been proposed for use in lieu of steel for reinforcement and prestressing tendons in concrete structures. The promise of FRP materials lies in their high-strength, lightweight, non-corrosive, non-conducting, and non-magnetic properties. Lighter weight materials and pre-assembly of complex shapes can boost constructability and efficiency of construction. At present, the higher cost of FRP materials suggests that FRP use will be confined to applications where the unique characteristics of the material are most appropriate. Efficiencies in construction and reduction in fabrication costs will expand their potential market.

1.4.2 Use of Glass Fibre Reinforced Polymer (GFRP) in Bridge Decks

GFRP has been used in deck slabs and steel free deck slabs, the cantilever overhangs (Black et al. 1997), traffic barriers (Benmokrane et al. 1998, Aly et al. 1997, Newhook and Mufti, 1996) and sidewalks (Rizkalla et al. 1998).

Prestressed concrete straps with GFRP as transverse confinement to steel free deck slab offer another example of the use of GFRP in bridges.

1.4.3 Prestressed Concrete Prisms

Prestressed concrete straps or prestressed concrete prisms (PCPs) have been used as structural elements. Svecova and Razaqpur (2000) describe PCP's use as flexural reinforcement in beams for the purpose of limiting deflection and crack width under service loads. Fensterwalder first used PCPs with steel strands for reinforcing pavements (Kommandigesellschaft & Kommandigesellschaft, 1963). Other uses of PCPs are in water tanks for delaying cracking, as reinforcement in lightweight concrete, as longitudinal reinforcement in pressured pipes, as vertical reinforcement for tanks and as transverse reinforcement for floors and roads.

The research reported in this thesis was undertaken to investigate the behaviour of steel free bridge deck confined laterally with prestressed concrete straps, under both static cyclic loading. In order to optimise the design of concrete straps, various developmental and confirmatory studies were undertaken, mostly with the help of full-scale laboratory models. The experimental work was limited to simple span structures.

Supplementary work was also initiated to understand the durability of GFRP bars in the alkaline environment of concrete.

Chapter 2

DESIGN OF PRESTRESSED CONCRETE STRAPS

2.1. General

The Canadian Highway Bridge Design Code (CHBDC, 2000) has the following mandatory conditions for the transverse confinement of steel free deck slabs (clause 16.7).

- The top flanges of all adjacent supporting beams are connected by an external transverse confining system, comprising straps that are perpendicular to the supporting beams and that they are either connected directly to the top of the flanges, as in welded steel straps, or connected indirectly, as in partially studded straps
- The spacing of the straps, S_l, is not more than 1.25 m
- The minimum area of cross-section of the strap, A in mm, is given by the following equation:

$$A = (F_s \times S^2 \times S_l \times 10^9) / (E \times t) \qquad (1)$$

Where, F_s = 6.0 and 5.0 MPa for external and internal panels, respectively; S is the girder spacing in m; S_l is the strap spacing in m; E is the modulus of elasticity of the strap material in MPa; and t is the slab thickness in mm. Of special note is the fact that the above equation relates to the axial rigidity of the strap and not to its strength.

- The direct or indirect connection of a strap to the supporting beams should have a shear strength of at least 200 A. These shear connecting devices are provided on the beam in the vicinity of the straps which are within 200 mm of the nearest strap. The commentary to the CHBDC explains that this requirement is basically for steel straps. For straps made of fibre reinforced polymers (FRPs), this requirement is expected to lead to conservative requirements for strap connection.

2.2. Initial Strap Size

Preliminary details of a concrete strap pretensioned with GFRP tendons are developed in the following for an external deck slab panel on girders at a spacing of 2.0 m. The composite slab is 175 mm thick, and the straps are proposed to be made with 35 MPa concrete. The modulus of elasticity of concrete is given by the following equation (8.4.1.7-CHBDC, 2000)

$$E_c = (3000\, f_c^{0.5} + 6900)\,(\gamma_c / 2300)^{1.5} \qquad (2)$$

When it is assumed that γ_c, the mass density of concrete, is 2500 kg/m^3, equation (2) gives E = 27932 MPa.

As noted in the previous section, the minimum strap spacing specified by the CHBDC is 1.25m. Assuming that the provision for minimum strap spacing was formulated on the basis of a clear minimum gap between the straps, the strap spacing is initially selected as 1.5 m. In light of the information given above, the area of the strap, can be calculated as:

$$A = (F_s \times S^2 \times S_l \times 10^9) / (E \times t)$$

$$A = (6.0 \times 2.0^2 \times 1.5 \times 10^9) / (27932 \times 175) = 7364 \text{ mm}^2 \qquad (3)$$

2.3. Design of GFRP Tendons

It is noted that equation (3) would have led to A = 1029 mm^2 for straps made of steel, for which the modulus of elasticity is 200,000 MPa. The connection strength, i.e. 200 A, is calculated by using this area, as the use of concrete area in equation (3) would lead to an unnecessarily high connection strength. The connection strength for the concrete strap = 200 x 1029 =205,800 N = 205.8 kN. In the light of this calculation, the maximum tensile force that the concrete strap will ever experience is 205.8 kN. It is noted that this estimate of the maximum tensile force, corresponding to the static failure load, is very conservative for the actual maximum factored wheel load, which is less than 25% of the static failure load of most deck slabs designed in accordance with the provision of the CHBDC. The factored load on two closely spaced wheels of a CL-625 Truck for the ultimate limit state, including impact, is 208

kN. Newhook and Mufti (1996) have measured strains in the straps of a full scale model of a steel free deck slab; their measured strains for a wheel load of 400 kN led to a tensile force of 50 kN in the strap. In order to be conservative, it is assumed that the maximum tensile force in the concrete strap would be twice the experimental force, i.e. 100 kN. It is noted that the strap force of 100 kN corresponds to a combined wheel load of about 800 kN, which is nearly 3.8 times the factored design load for the ultimate limit state.

In order to keep the concrete of the strap always free from any cracks, it should be prestressed with a minimum force of 100 kN. It is hypothesised that the transverse confinement to a steel-free deck slab (Mufti et al., 1993; Newhook and Mufti, 1996) can also be provided externally by means of concrete straps, which are kept from cracking by means of prestressing. The prestressing can be provided through steel or FRP tendons. Some attributes of the various tendons are noted in the following.

Steel Tendon: The steel is initially protected against corrosion by the alkalinity of concrete, usually resulting in durable and serviceable condition. For structures subjected to aggressive environments, such as marine structures, bridges and parking garages exposed to deicing salts, combinations of moisture, temperature, and chlorides reduce the alkalinity of the concrete and result in the corrosion of reinforcing and prestressing steel. The corrosion process ultimately causes concrete deterioration and loss of serviceability. To address corrosion problems, engineers have turned to alternative metallic reinforcement, such as epoxy coated steel bars. While effective in some situations, such remedies may still be unable to completely eliminate the problems of steel corrosion (Keesler and Powers, 1988).

Steel tendons are the least expensive, however, prestress losses in thin concrete elements are large owing to their high stiffness ratio. The laboratory studies carried out at Queen's University by Batchelor et al., (1982) showed that the stiffness ratio of the prestressed deck system has a direct bearing on the loss of prestress. Higher stiffness ratios cause higher losses.

The stiffness ratio R_k is given by the following expression:

$$R_k = \frac{k_p}{k_e} \tag{4}$$

Where

$$k_p = \frac{E_p A_p}{L_p} \quad \text{and} \quad k_e = \frac{E_c A_c}{L_c} \tag{5}$$

k_p and k_c denote the stiffness of the prestressing system and the concrete respectively. E_p, A_p and L_p are modulus of elasticity, sectional area and length of the prestressing system respectively; and E_c, A_c and L_c are modulus of elasticity, sectional area and length of the concrete strap respectively. Bakht and Jaeger (1994) have given the loss of prestress δP, as follows:

$$\delta P = P\left(\frac{1-\alpha}{1+\frac{\alpha}{R_k}}\right) \tag{6}$$

Where, α represents the fractional decrease in the stiffness of the deck.

It is apparent from the above equation that though steel is the customary option owing to its easy availability and low cost, but due to its corrodible nature and high prestress losses its use is only limited as a control specimen in this research. To minimise the prestress losses a low-modulus and high-strength material is required.

Use of Fibre Reinforced Polymers

Several countries, such as Japan (JSCE 1997) and Canada (CSA 2000), have established design procedures specifically for the use of FRP reinforcement for concrete structures. In the USA, the analytical and experimental phases are sufficiently complete and efforts are being made to establish recommendations for design with FRP reinforcement.

Aramid Tendons: Compared to high strength steel, aramid fibre rope has 75% more strength, and its modulus of elasticity is only 41% that of the high strength steel. In addition to being a high-strength low-modulus fibre, it is also flexible and non-corrosive. A prototype timber bridge was built using aramid fibre rope PARAFIL for lateral prestressing. It was reported that there was virtually no loss of prestress even after more than two and a half years. However this system could not be exploited commercially due to high initial cost of the rope and the special anchorage system Bakht et al. (1997).

Carbon Fibre Reinforced Polymer Tendon (CFRP): CFRP tendons have the highest tensile modulus of elasticity amongst the various FRP's, typically more than 50 percent of the modulus of steel. CFRP tendons are suitable in aggressive environments but are very expensive and suffer high prestress losses owing to their high modulus of elasticity. Therefore, CFRP was not used as a prestressing element in this research.

GFRP Tendons: There are two main types of fibres used for GFRP, namely, E-glass, which was originally developed for electrical applications, and S-glass, which was developed for structural applications. There is a new type of glass fibre introduced in the market called Z-glass, with the claim of high resistance to alkalis. E-glass and S-glass have a modulus of elasticity of 60 GPa and tensile strength of 2400 MPa (CHBDC, 2000).

GFRP tendons are not as expensive as CFRP tendons; they are suitable in aggressive environments, but are permitted to be used only if the pretensioned components are made with non-alkaline concrete (CHBDC, 2000). Because of their low modulus of elasticity, GFRP tendons suffer very little prestress losses.

Benmokrane and Masmoudi (1996) have cited the following properties for GFRP C-bars of 14.9 mm diameter.

Average tensile strength	= 773 MPa
Standard deviation of tensile strength	= 53 MPa
Average modulus of elasticity	= 37,650 MPa

From the above properties, the 5th percentile tensile strength is 686 MPa. The CHBDC (2000) permits a maximum jacking stress of 55 % of the 5th percentile tensile strength in GFRP tendons, or 377 MPa. The required area of cross-section of GFRP tendons to sustain a tensile force of 100 kN, is 265 mm^2. The two # 5 GFRP bars, each with a diameter of 14.9 mm, provide a total cross-section of 349 mm^2. These bars, stressed at 377 MPa, would provide a total tensile force of 132 kN. It is expected that even after prestress losses, the net tensile force in the tendons would remain well above the design value of 100 kN.

Since the Elastic Modulus of concrete is of the same order of magnitude of the GFRP bars, there is no need to correct the stiffness of the strap to account for the slightly higher modulus of elasticity of GFRP bars.

2.4. Final Size of Strap

For a GFRP tendon with a diameter of about 15 mm, and a cover of 40 mm (CHBDC, 2000), the minimum thickness of the concrete strap is 95 mm, say 100 mm. As shown

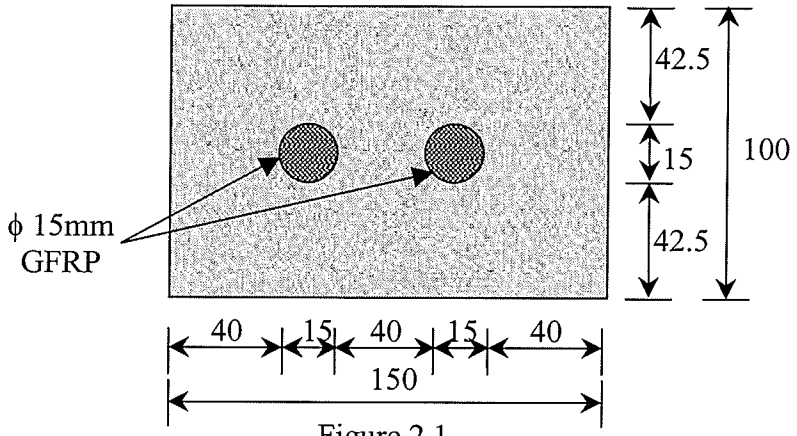

Figure 2.1
Cross-section of Strap

in figure 2.1, the minimum cover requirement forces the width of the concrete strap to be at least 150 mm, thus providing an area of 15000 mm^2, more than twice the required value of 7364 mm^2. It is obvious that this strap can be placed at a spacing of 3.0 m, if such spacing was permissible.

2.5. Connection to Girder

As calculated in section 2.2, the minimum required shear strength of the strap connection to the girders is 205.8 kN. It was decided to provide the connection with the help of double-headed shear studs. The CHBDC (2000) requires the factored shear resistance of a headed shear stud, q_r, to be calculated from the following equation –

$$q_r = 0.5\varphi_{sc} A_{sc} (f_c' E_c)^{0.5} < \varphi_{sc} F_u A_{sc} \qquad (6)$$

Where ϕ_{sc}, the resistance factor = 0.85; A_{sc} is the cross-sectional area of the stud; f'_c and E_c are the compressive strength and modulus of elasticity of concrete, respectively; and F_u is the minimum tensile strength of steel stud, taken as 350 MPa. For a 20 mm diameter stud, the two expressions on the right-hand side of equation (6) give 131 and 93 kN, respectively. Choosing the latter value leads to 3 shear connectors.

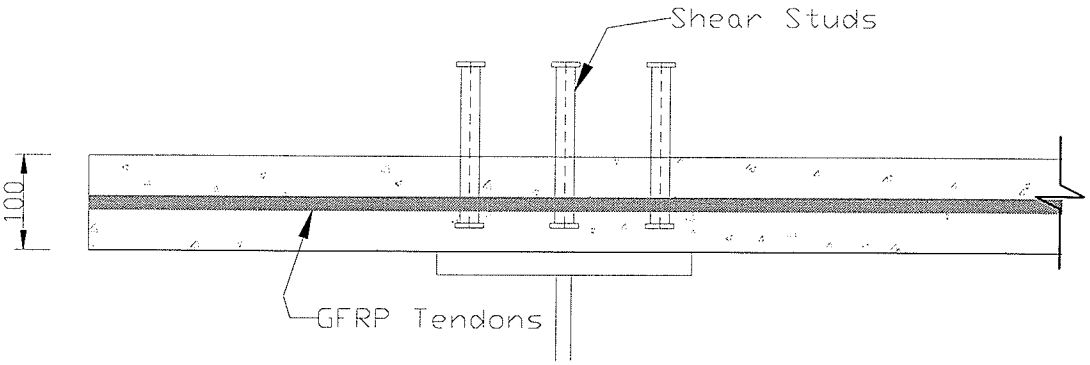

Figure 2.2
Partially Studded Strap

The use of prestressed concrete straps with shear studs above the girders as transverse confinement illustrated in figure 2.2, is based on the idea of partially studded strap, and it being noted that the strap is subjected to mainly axial tensile force.

The rationale behind the selection of a double-headed shear connector is the fact that in steel-concrete composite beams, the concrete in the slab is able to withstand the transfer of interface shear through the stems and heads of the shear

studs. It is, therefore, concluded that the concrete in the strap should also be able to sustain the calculated shear force through the stems and heads of its three shear connectors.

2.6. Required Research

In order to put to practice the concept outlined in the above sections, various developmental and confirmatory studies were undertaken with the help of full-scale laboratory models as detailed in the following:

Assessment of the Stiffness of the Straps

The proposed concept is based on the premise that a concrete prismatic member in tension retains its full axial rigidity, provided that the applied force does not exceed the prestressing force. This premise was explored quantitatively with the help of tensile tests on the following specimens; each with a length of 1500 mm between the grips and each constructed with concrete made of Portland cement.

- Three 100 x 150 mm concrete straps reinforced with two 20 mm diameter steel bars.
- Three 100 x 150 mm concrete straps pretensioned with two 15 mm diameter GFRP bars, each bar stressed with 55% of the 5^{th} percentile tensile strength.
- Three 100 x 150 mm concrete straps pretensioned with two 15 mm diameter GFRP bars, to be tested three years after casting

The first two sets were tested soon after casting to determine if the concrete strap can develop sufficient axial rigidity even if the prestressing is partially or totally absent. The third set was proposed to study the effect of loss of prestress as well as to study the deterioration of the GFRP bars in an alkaline environment of concrete. Investigation of the last mentioned set is beyond the scope of the research mentioned herein.

Chapter 3

ASSESSMENT OF TENSILE STRENGTH OF GFRP BARS

3.1. Introduction

It was decided to prestress the concrete straps with GFRP tendons. C-Bar manufactured by Marshall Industries Composites Inc. was chosen. For # 5 bar, the manufacturer quoted the following properties.

Mean Tensile Strength	= 680 MPa
Standard Deviation of Tensile Strength	= 22 MPa
Average Modulus of Elasticity	= 42 GPa

Although the value of ultimate tensile strength, f_{pu} is obtained from the manufacturer, it needs to be confirmed by a test method, as there is little uniformity between the various test methods currently being used for FRPs.

Annex B S806-00 specifies an anchor for FRP reinforcement specimens to facilitate their gripping for various types of tests carried out under tensile loading.

3.1.1 Handling, Storage and Placement

Because FRP tendons can be damaged during handling, special precautions were needed for their handling and placement. FRP components were protected from damage during unloading, as they are less robust than their steel counterparts. Care was exercised not to cause damage by trampling and bending them. The cutting of the FRP bars was done with the help of a high-speed cutter. Prior to testing, the specimens were conditioned for a fortnight at a temperature not exceeding 20°C.

3.1.2 Capacity of Anchors

Anchors should be capable of developing at least 90% of the specified tensile strength of the FRP tendon (CHBDC, 2000). Anchors having considerably smaller capacity than the tendons are likely to be inefficient, in that they may overstress some fibres, which could cause premature failure of a tendon. Most GFRP reinforcement on the market is proposed for non-prestressed applications and since GFRP has very low transverse shear strength, manufacturing of prestressing anchorages for GFRP bars are difficult. (Erki and Rizkalla, 1993)

3.2. Geometry of Anchor and Specimen Preparation

A resin sleeve-type anchor using a steel pipe and a low viscosity epoxy was used in this study. The steel pipe used was a readily available inexpensive pipe used in plumbing. The dimensions of the anchor are shown in figure 3.1. The geometric characteristics of the steel sleeve were in accordance with Annex B S806-00.

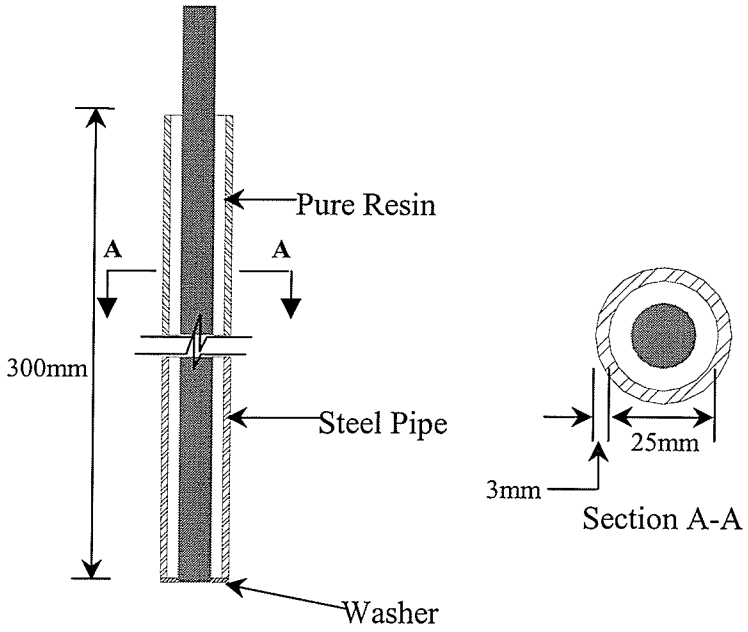

Figure 3.1
Anchor Details

The anchor sleeves had a thickness of 3 mm, the inner diameter of 25 mm and a length of 300 mm at each end. Four 1.2 m long GFRP rods were tested in tension.

3.2.1 Anchor Casting Procedure

The anchors were cast in vertical position. The anchors were thoroughly cleaned first with a wire brush and then with soap and water. The bar was held axially inside the cylinder before the cylinder was filled with resin. Washers were glued onto the ends of the anchors to align the bars concentrically to the anchors. A jig was specially made to hold the anchors and the specimen, axially aligned.

The sleeve was filled with WEST SYSTEM® Brand Epoxy 105/205 in an upright position. The resin was mixed and handled in accordance with the manufacturer's instructions. The specimens were allowed to cure for a minimum of 24 hours before testing. The anchored specimens were handled by holding both grips, in order to avoid bending or twisting.

3.3. Test Setup and Results

The bars were instrumented with strain gauges in the longitudinal as well as lateral direction to evaluate the ultimate tensile strength, modulus of elasticity and the Poisson's ratio. The strains were monitored with the aid of a data acquisition system, which consisted of a Data General Conditioner Rack and a Labview 6.0. The test setup can be seen in figure 3.2. It was observed that the GFRP bars failed in the gauge length portion, well away from the anchors (Figure 3.3). The stress-strain diagram for one of the bars is shown in figure 3.4; it can be seen that, as expected, the stress-strain curve is linear.

The measured mechanical properties of the GFRP bar are as follows-

Average ultimate tensile strength	= 886 MPa
Modulus of elasticity	= 41.15 GPa
Standard deviation	= 21.8 MPa
Poisson's ratio	= 0.277

Coefficient of variation of tensile strength = 0.0246

It can be seen that while the measured modulus of elasticity and the standard deviation matches very well the manufacturer's prediction, the actual tensile strength is much higher.

To verify the specified tensile strength with the above test, the average test strength of the specimens is multiplied by the factor F_t (Jaeger and Bakht, 1993), and this product must be at least equal to the specified tensile strength. The factor F_t depends upon the coefficient of variation of the tensile strength V_{FRP}, and the number of test specimens, n, and is given by the following:

$$F_t = \frac{1 - 1.65V_{FRP}}{1 + 1.65V_{FRP}/\sqrt{n}} \quad (1)$$

If n is more than 10, the value of V_{FRP} is either obtained from test results or the value supplied by the manufacturer. In our case the number of specimens was four, therefore the average ultimate tensile strength is multiplied by the factor F_t, which was found out to be 0.959.

Henceforth, the average ultimate tensile strength is taken as 849 MPa

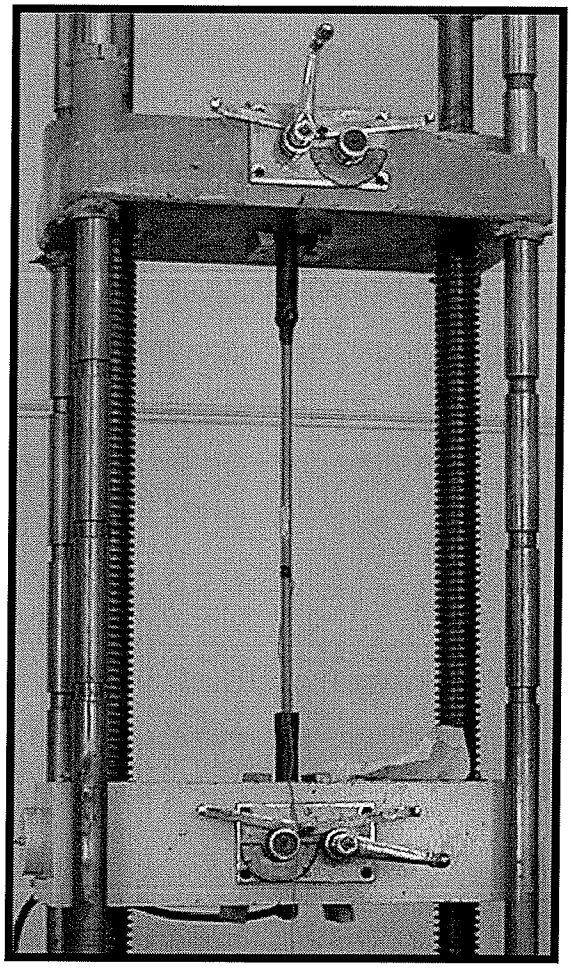

Figure 3.2
Test Set-up

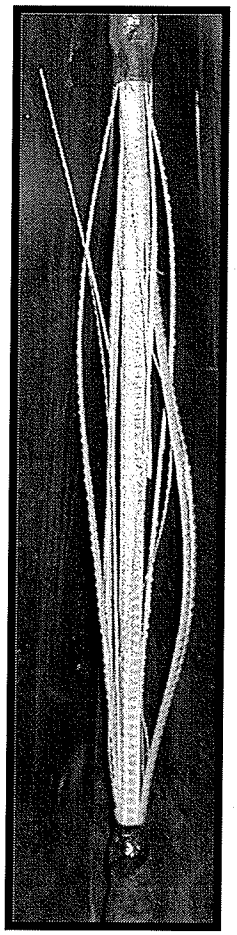

Figure 3.3
GFRP Rupture

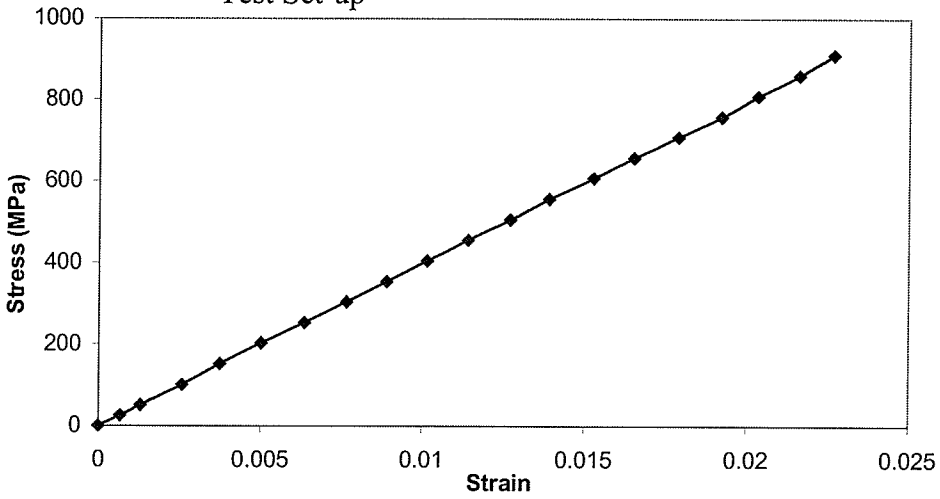

Figure 3.4
Stress-Strain Diagram for GFRP bar

Chapter 4

RATIONAL MODEL FOR PREDICTING THE CRACKING LOAD OF CONCRETE STRAPS

Two types of rectangular straps were considered in this thesis, straps with non-prestressed reinforcement in one case and prestressed tendons in the other. It will be assumed that the concrete is subjected to strains in only the axial direction and that these concrete strains are uniform over the cross-section.

4.1. Compatibility Conditions

The concrete strain is taken to be zero when the concrete is cast. Thus, the length of the member at the time of casting is defined as the undeformed length of the member, L. The axial deformation measured from this undeformed condition will be denoted by Δ as shown in figure 4.1. The concrete strain, which is assumed to be uniform both over the cross-section and along the length of the member is given by

$$\varepsilon_c = \frac{\Delta}{L} \qquad (1)$$

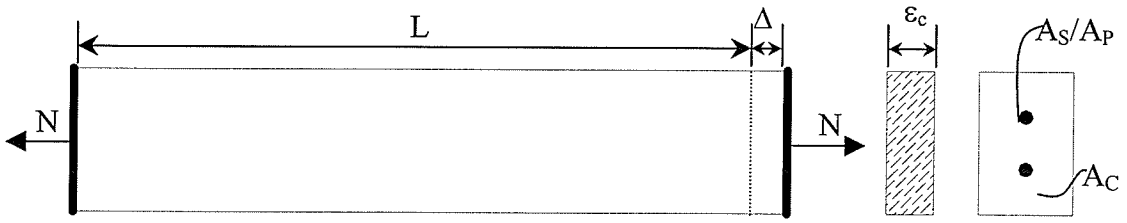

Figure 4.1
Member Subjected to Axial Load

We will assume that the concrete, the reinforcing bars or the prestressing tendons are all rigidly anchored at the ends of the member. Hence, any change in

length of the concrete must be accompanied by an identical change in length of the reinforcement.

The non-prestressed reinforcement and the concrete both have zero strain at the time the concrete is cast. As these two materials start with the same strain, have the same undeformed length, and undergo identical deformations, their strains must always be equal. Hence

$$\varepsilon_s = \varepsilon_c \tag{2}$$

Because prestressing involves stretching the reinforcement, the prestressed reinforcement does not start with the same strain as the surrounding concrete. Furthermore, the prestressed reinforcement will have a somewhat shorter (by about 1%) undeformed length than the surrounding concrete. While the two materials start with different strains, they will subsequently be subjected to identical changes in deformation. Hence, the subsequent changes in strain can be considered to be identical (the small difference in undeformed lengths is ignored). Thus, the difference in strain between the prestressing steel and the surrounding concrete will essentially remain constant throughout the life of the member. This strain difference, $\Delta\varepsilon_p$, is the basic "signature" of the prestressing operation. Hence, at any stage in the life of a prestressed member, the strain in the prestressed reinforcement can be found from the strain in the surrounding concrete as

$$\varepsilon_p = \varepsilon_c + \Delta\varepsilon_p \tag{3}$$

The strain difference, $\Delta\varepsilon_p$, can be determined from the specific details of the prestressing operation. For pretensioned members the concrete strain in zero, while the strain in the prestressing tendons, ε_{pbed}, has a high tensile value when the two materials are bonded together as shown in figure 4.2. Hence, for pretensioned members the strain difference is equal to the tensile strain in the tendons at the time the concrete is placed.

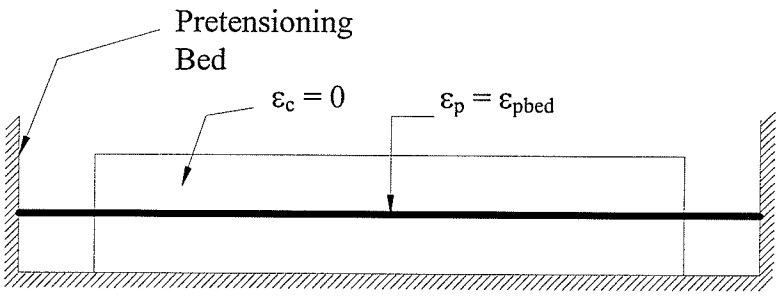

$$\Delta\varepsilon_p = \varepsilon_p - \varepsilon_c = \varepsilon_{pbed}$$

Figure 4.2
Calculation of Strain Difference, $\Delta\varepsilon_p$

4.2. Equilibrium Conditions

The required equality between the internal stresses and the applied load, N leads to the following equation.

$$\int_A f dA = N \tag{4}$$

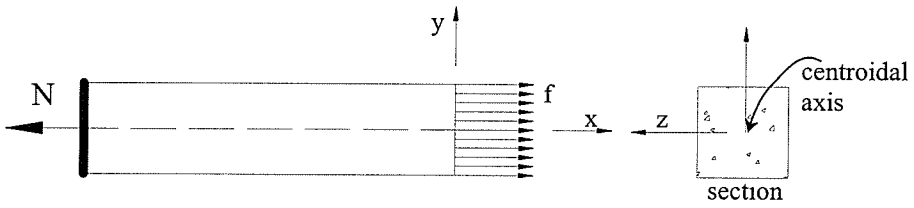

Figure 4.3
Free-body Diagram of Member Subjected to Axial Load

As the total concrete strain is uniform and assuming that the temperature and shrinkage strains are uniform, the stress in the concrete will be uniform over the section. Similarly, the reinforcing bars or the prestressing tendons will all have the same stress. The above equation can be transformed into the following equation.

$$A_c f_c + A_s f_s = N$$

or

$$A_c f_c + A_{frp} f_{frpp} = N \tag{5}$$

Where, A_c, A_s, A_{frp} are the areas of concrete, steel reinforcing bars and FRP tendons respectively. f_c, f_s, f_{frp} are the stresses in concrete, steel reinforcing bars and FRP tendons respectively, as shown in figure 4.3.

4.3. Predicting Response of Axially Loaded Members

The response of uniformly strained elements can be predicted by using the equilibrium and compatibility conditions, together with the material stress-strain relationships.

In calculating the response of these elements, short term loading (i.e. negligible creep effects) and zero shrinkage and temperature strains are assumed. For concrete in compression, simple parabolic stress-strain relationship is considered and for concrete in tension, the equation specified by Carreira and Chu (1986) is employed.

To determine the complete load-deformation response, we determined the axial load, N, which corresponds to various values of compressive and tensile strains in the concrete, ε_c and ε_t. The procedure was to choose a value of ε_c and ε_t, to find the corresponding strains in the reinforcing bars or the prestressing FRP tendons, to find the stresses corresponding to these strains using appropriate stress-strain diagrams, and then finally to calculate the corresponding axial load, N.

Throughout the calculations, the convention followed is that the tensile stresses and tensile stresses are positive while compressive stresses and compressive strains are negative (Collins and Mitchell, 1997).

4.3.1. Concrete in Uniaxial Compression

While the compressive stress-strain responses of the constituents of the concrete are linear, the stress-strain response of concrete is non-linear. The non-linearity of the concrete stress-strain response is caused by the interaction between the paste and the aggregate. Microcracks occur at the aggregate-paste interfaces at

relatively low stress levels. The development and propagation of these cracks soften the concrete, resulting in a non-linear stress-strain curve.

For concrete strengths less than about 41 MPa (6000 psi) the stress-strain relationship can be reasonably described by a simple parabola (Collins and Mitchell, 1997). That is,

$$\frac{f_c}{f_c'} = 2\frac{\varepsilon_c}{\varepsilon_c'} - \left(\frac{\varepsilon_c}{\varepsilon_c'}\right)^2 \qquad (6)$$

Where f_c' = peak stress obtained from a cylinder test

ε_c' = concrete strain at peak stress

ε_c = strain in concrete corresponding to f'_c

f_c = stress in concrete corresponding to ε_c

4.3.2. Concrete in Uniaxial Tension

It is difficult to test concrete in pure axial tension; therefore, the cracking strength is usually determined from an indirect test. Typically, either the modulus of rupture, f_r, is determined from a bending test, or the splitting strength, f_{sp}, is determined by splitting a concrete cylinder with a line load. The double-punch test is an indirect test method for determining concrete cracking strength, however this test is seldom used.

The tensile stress at which concrete cracks is not constant for a particular concrete but varies with a number of parameters. Increasing the volume of concrete subjected to high tensile stress lowers the cracking stress. Hence, larger members crack at lower stresses. Additional factors such as the presence of restrained shrinkage stresses can greatly reduce the apparent cracking stress. Therefore, the stresses determined from the various test methods would differ.

If only the concrete cylinder crushing strength, f_c', is known, then an estimate of the direct cracking strength f_{cr} can be made using equation 7 (CSA A23.3-94)

$$f_{cr} = 0.33\lambda\sqrt{f_c'} \quad \text{(MPa)} \tag{7}$$

Where λ = factor accounting for the density of concrete

= 1.00 for normal weight concrete

Testing of concrete in direct tension was not feasible; instead split cylinder test was done in the laboratory to evaluate the direct cracking strength of concrete. As per ASTM C-496, splitting tensile strength can be calculated as follows

$$f_{sp} = 2P / \pi ld \tag{8}$$

Where,

f_{sp} = splitting tensile strength

P = maximum applied load indicated by the testing machine

l = length of the concrete cylinder

d = diameter of the concrete cylinder

Based on the split cylinder test, the direct cracking strength can be estimated as (Collins and Mitchell, 1996) –

$$f_{cr} = 0.65 f_{sp} \tag{9}$$

4.3.2.1.Stress-Strain Relationship for Reinforced Concrete in Tension

The shape of the concrete stress-strain diagram in tension depends heavily on the testing procedure used. When plain concrete is tested in direct tension, using a testing machine in which the strain rate cannot be controlled, a linear diagram with a brittle failure is usually obtained.

Experiments have shown that if the strain rate is controlled, the stress-strain diagram of plain concrete in tension is non-linear and has well defined ascending and descending branch (Carreira and Chu, 1986). It was necessary to correctly formulate the stress-strain relationship of concrete in tension to calculate the corresponding axial load, N and later it would be seen that the analytical relationship formulated in this section is used to compare it with the experimental load-strain behaviour of the prestressed concrete strap.

The same general form of the serpentine curve used for the complete stress-strain relationship in compression is also employed for the average stress-strain diagram of reinforced concrete in tension (Carreira and Chu, 1986). The average diagram represents the overall or resultant behaviour of concrete in tension restrained by reinforcement.

$$\frac{f_t}{f_t'} = \frac{\beta\left(\varepsilon/\varepsilon_t'\right)}{\beta - 1 + \left(\varepsilon/\varepsilon_t'\right)^{\beta}} \qquad (10)$$

where,

f_t = the stress corresponding to the strain $\varepsilon = g_1(wf'_c)^{0.5}$

f'_t = the point of maximum stress, considered as the tensile strength

ε'_t = the strain corresponding to the maximum stress f'_t

β = a parameter that depends on the shape of the stress strain diagram

Design Parameters used with the Proposed Equation

The above mentioned parameters were not experimentally evaluated in this research but the values suggested by the researchers, Carreira and Chu (1986) were employed.

- **Concrete Tensile Strength**

The direct tensile strength of plain concrete is conservatively given as –

$$f'_t = g_1\sqrt{(wf'_c)} \qquad (11)$$

Where,

$g_1 = 0.0069$

w = concrete unit weight in kg/m^3

f'_c = concrete compressive strength

- **Tensile Strain ε'_t**

The value of ε'_t was approximated for normal weight concrete as 0.00018

- **Estimating the Value of β in Tension**

The value of β used in this analytical study was 2.0

Chapter 5

EXPERIMENTAL INVESTIGATION OF AXIAL STIFFNESS OF CONCRETE STRAPS

5.1 Experimental Investigation of Axial Stiffness of Reinforced Concrete strap

5.1.1 Description of Experimental Model

An experimental program was undertaken at the University of Manitoba to examine the behaviour of concrete straps reinforced with steel bars subjected to axial tensile forces. Three concrete straps reinforced with steel were cast in the concrete laboratory at the University of Manitoba. The length of the strap between the anchors was 1500 mm and the length of the anchors was 300 mm. The strap was reinforced by two 20 mm diameter deformed steel bars, and the anchorage zone consisted of six 12 mm diameter threaded steel rods and LCC-0.092 wire mesh at either end to control

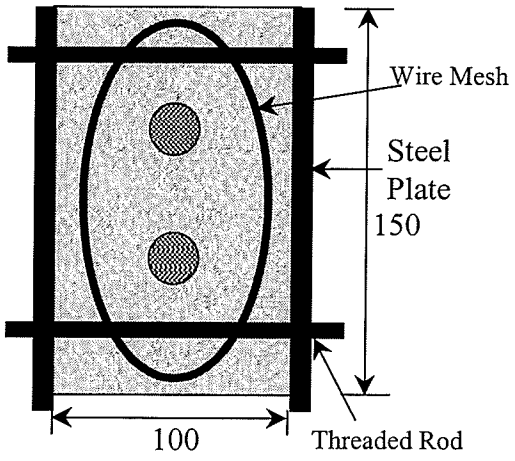

Figure 5.1
Anchorage Zone Cross-section

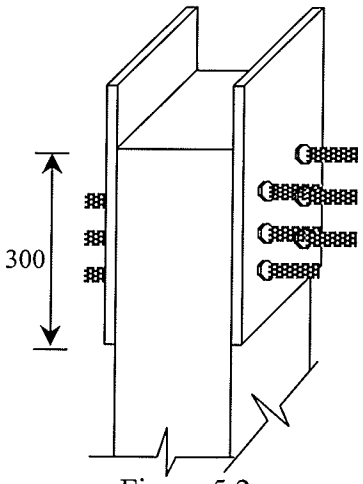

Figure 5.2
Anchorage Zone

the bursting and splitting stresses. The cross-section through the anchorage zone is shown in figure 5.1.

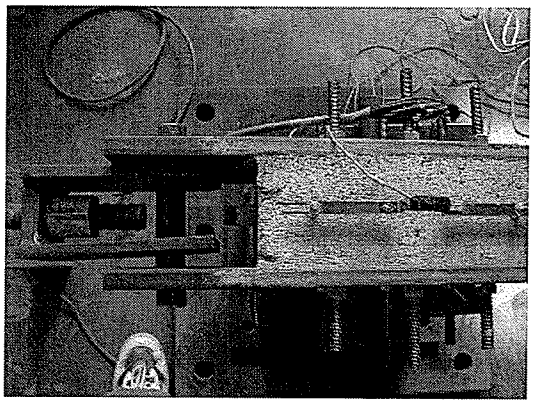

Figure 5.3
Pulling Mechanism

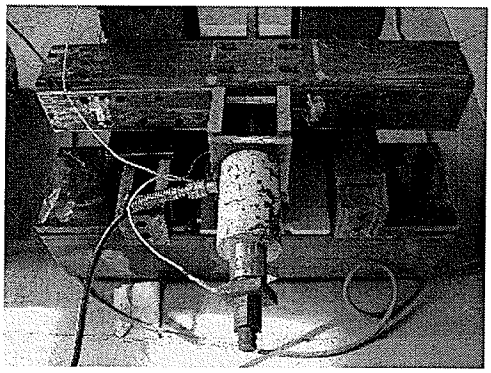

Figure 5.4
Jacking End

The strap was gripped with two 20 mm thick steel plates as shown in figure 5.2, which were roughened on the inside to have a better bond with the concrete. The steel plates were pulled with a 32 mm diameter dywidag bar using a steel coupler as shown in figure 5.3. The dywidag bars were pulled against bulkheads, thus applying tensile force to the straps as shown in figure 5.4.

The concrete was designed for a 28-day strength of 40 MPa and prepared in the laboratory. The mixer used for this project had a capacity of 0.085 m^3 (3 cubic feet), prompting us to prepare two batches, as the volume of concrete needed for one strap was about 1.25 cubic feet. 10 mm coarse aggregate was used to satisfy the criteria for the minimum clear spacing between the reinforcing bars.

The mix design and mechanical properties of the concrete used in the straps are given in table 5.1, it being noted that the mechanical properties were obtained from tests on six cylinders.

Table 5.1:Concrete Mix Design and Properties

Component	Value
Type 30 Cement	500 kg/m^3
Water	200 kg/m^3
Coarse Aggregate	1034 kg/m^3
Fine Aggregate	620 kg/m^3
Slump	95 mm
Density	2417 kg/m^3
Compressive strength (average)	40.76 MPa
Elastic modulus (average)	28785 MPa

5.1.2 Description of Instrumentation

The steel bars were instrumented by electrical resistance strain gauge on seven locations along the length of the bar, to gauge the profile of the strain. Using the appropriate mathematical expressions, the strains were converted to stresses and subsequently multiplied by the cross-sectional area to calculate the axial force. The concrete straps were instrumented with PI gauges (Figure 5.5) to measure the crack width and linear variable displacement transducers (LVDTs) to measure the elongation.

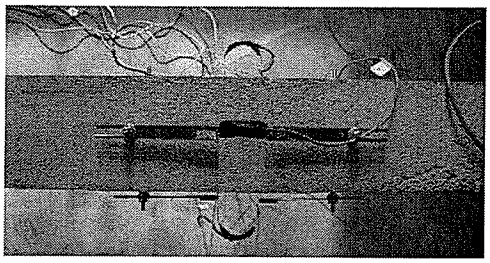

Figure 5.5
PI-Displacement Transducer

In all tests, the load was applied using hydraulic jack that had a capacity of 10000 psi. Load was monitored with the help of load cell with a capacity of 330 kN (75000 lbs.). The jack and the load cell were calibrated prior to the actual testing. All the instruments were connected to a data acquisition system.

5.1.3 Testing Procedure

Each strap was first subjected to 50 cycles of gradually increasing axial tensile load of 50 kN, and then tested until failure. Initially the straps were tested on the structural floor with the ends of the strap resting on rollers to reduce the frictional resistance, but the set-up was later elevated to better view and plot the crack patterns on the strap. After the fatigue test, the strap was taken to failure by applying a steadily increasing load and crack patterns were observed at each load step. A typical pattern of cracking will be presented and discussed later in the chapter. The load was increased until the ultimate capacity was reached. Ultimate load carrying capacity was characterised in each strap by the failure of the anchorage zone.

For the first strap, the ultimate test had to be repeated thrice in lieu of the failure of the pin, which connected the strap to the pulling mechanism. Due to the substantial cracking resulting from several tests, the stiffness of the first strap was smaller as compared to other straps.

5.1.4 Observed cracking behaviour during testing

During the cyclic loading as well as the ultimate loading, the RC straps exhibited a characteristic sequence and pattern of cracking. The sequence can be described by the following progression of cracking.

- Within 5 cycles, primary cracks developed, followed by extension of theses cracks as the number of cycles increased.
- Crack depth decreased linearly with decreased crack spacing

Figure 5.6 shows a photograph of the crack pattern of strap III after the steel bars in the strap had yielded. The pattern of cracking for the other two bars was very similar to the one shown in the photograph.

Failure of the strap was in the anchorage zone accompanied by an enormous noise, due to the slipping of the steel bars through the anchors. It would be seen later that, though the failure was not in the desired location, the steel bars yielded before this failure took place.

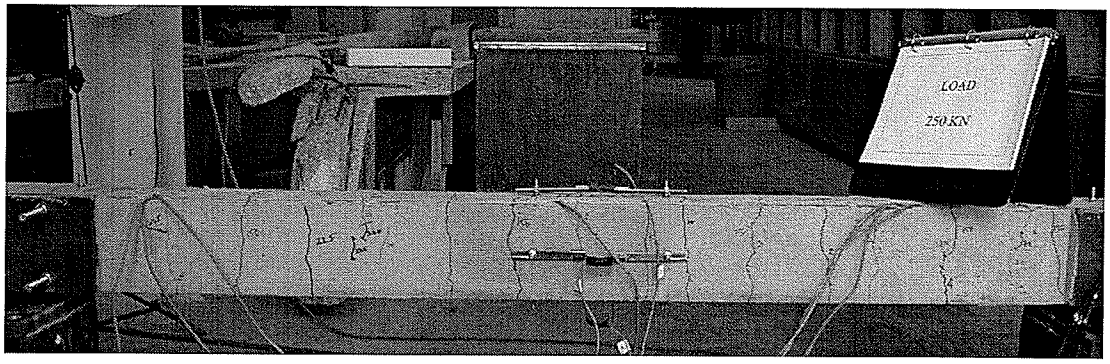

Figure 5.6
Crack Pattern at 250 kN – Strap III

5.1.5 Load-Strain Results

The measured load-strain histories for the cyclic loading for one of the straps are shown in figure 5.7 for cycle number 1, 25 and 50. As can be seen from the graph, the load strain curve for a complete cycle forms a hysteresis loop. The first cycle leaves a small residual strain. In subsequent cycles, the residual strain continues to be

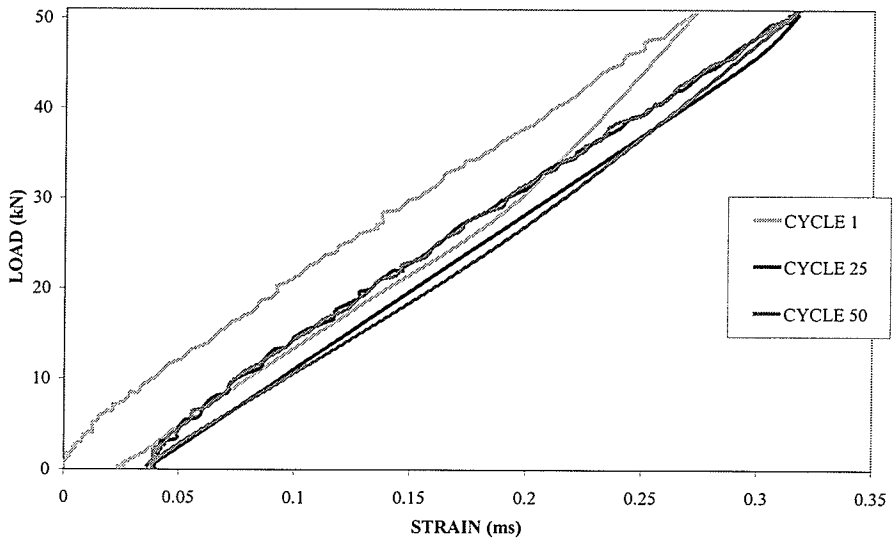

Figure 5.7
Cyclic Loading – Strap III

reduced until the strap reaches a stable and elastic state. For load cycle one, the change in response is quite large but by load cycle twenty-five, the strap had stabilized considerably, and for cycle fifty, there was no residual strain.

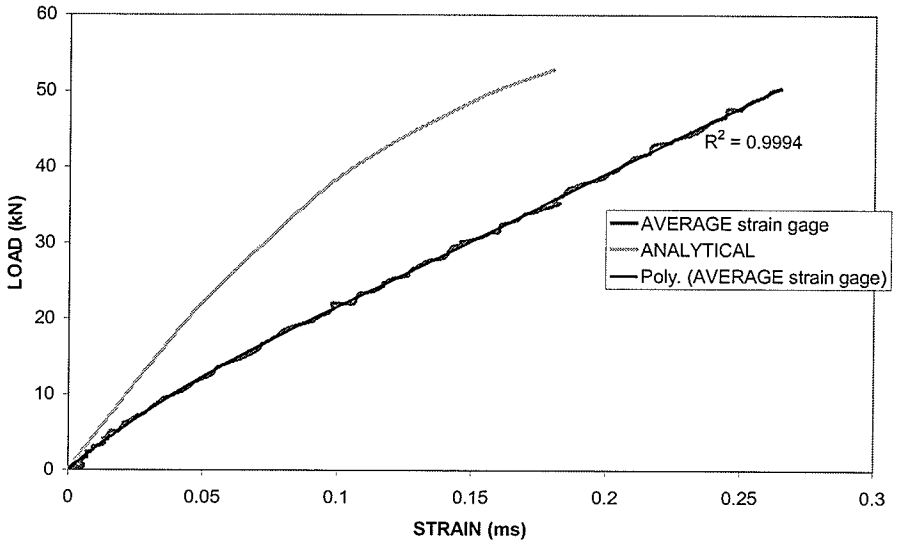

Figure 5.8
First Cycle of 50 kN – Strap III

In figure 5.8, load-strain curve of cycle one for strap I is being compared to the curve calculated from the analytical model as described in the previous section. At a first glance, the slope looks essentially linear, negating the theory that, stress-strain relationship for concrete in tension is non-linear (Carreira and Chu, 1986). But on closely examining the curve, with the help of regression analysis or the R-squared term, it was found that the R-squared term had a better accuracy with the polynomial trend line rather than a linear trendline. The slope of the polynomial trendline is convex which is similar to that of the analytical model, although, there is an obvious discrepancy between the two curves, which can be attributed to the loading mechanism. If the loading had been strain controlled, the slope would have been very similar to that of the analytical model.

As mentioned previously, the experimental determination of the parameters f'_t, ε'_t and β, which could have influenced the analytical curve were beyond the scope of this thesis.

On extending the load-strains curve to its their whole range, i.e. to its ultimate failure load, it can be seen that when the reinforcing bars embedded in concrete are stressed in tension, the concrete assists the reinforcement in carrying the tensile force, even after severe cracking has developed (Figure 5.9). The concrete contribution after cracking is referred to as tension stiffening by concrete or simply tension stiffening. The reason for having strain rather than elongation in the x-axis was to observe the yielding strain in the steel bars.

One other interesting observation from the above graph is the load-strain performance of strap 1, due to the fact that the tension tests were done thrice on this strap, due to test set-up deficiencies, the stiffness had greatly reduced.

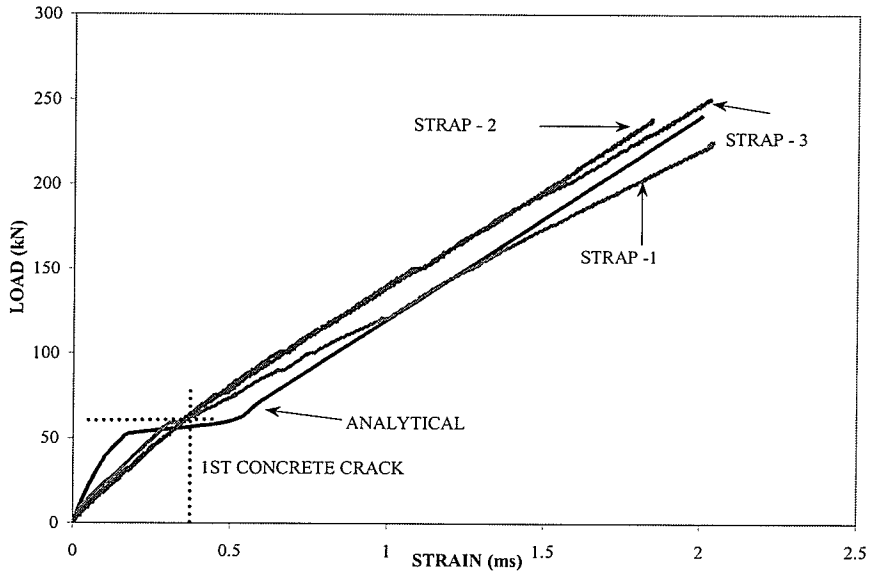

Figure 5.9
Ultimate Failure Load of the
Three Straps

5.1.6 Comparative Axial Stiffness- Steel Strap vs RC Strap

In all applications of the FRC slab, the straps have been made of steel. Typically, these steel straps, are 50×25 mm in cross-section and are made of 300W steel. Understanding the fact that, load-elongation plot for steel would remain essentially linear until yielding, an experimental test was not performed on the steel strap. A graph is however plotted in figure 5.10 that compares the theoretical axial stiffness of a steel strap with the measured axial stiffness of a reinforced concrete

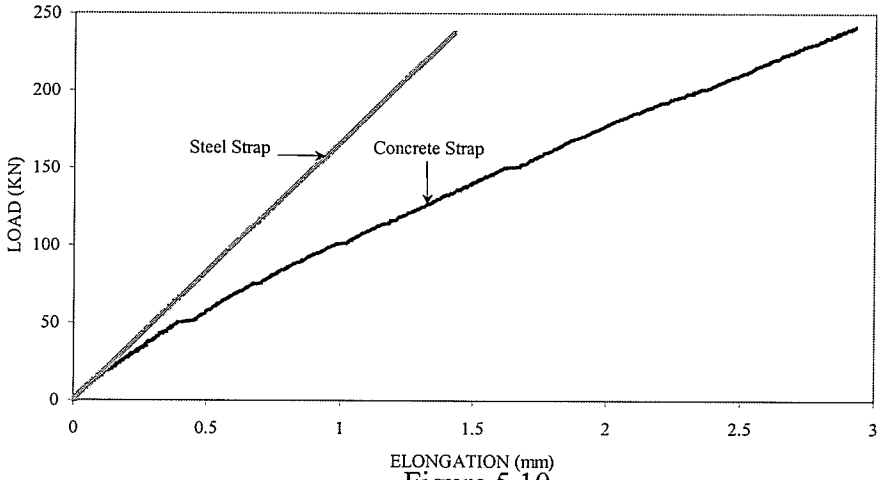

Figure 5.10
Comparative Axial Stiffness

strap. It can be seen from the graph that the stiffness of the reinforced concrete strap reduces substantially, once the concrete cracks. It is obvious that the concrete needs to be prestressed to avoid cracking at a very early load.

The plot of the elongation was calculated for a gauge length of 1500 mm of the strap.

5.1.7 Inference

The commentary in the CHBDC, 2000 Cl-16.7 describes that the straps are required for their axial stiffness and not for their strength. Since, the stresses induced in the straps are expected to be small under service loads, therefore, their fatigue resistance is not of concern. As it was observed that the stiffness of the reinforced concrete straps decreases by 50% after cracking, it was decided to experimentally assess the stiffness of prestressed concrete (PC) straps with GFRP.

The following lessons were learnt from tests on reinforced concrete straps, to be improved upon in the future tests involving tension tests on PC straps.

- Anchorage zone – As the failure was due to the steel bars in the straps slipping out of the anchors, more reinforcement and increased length of the anchorage zone was needed to curtail this behaviour. When the embedment length becomes long enough, the bar will yield in tension or rupture before it pulls out of the strap.

- Refined instrumentation – To monitor the slip, if any, between the concrete and the anchorage zone, additional instrumentation was needed
- The results from the PI gauges that were installed in the anchorage zone were neglected, as there was slippage at the ends due to stress transfer, resulting in lower strain values.

5.2. Experimental Investigation of Axial Stiffness of Prestressed Concrete Strap

5.2.1. Introduction

An experimental program was undertaken to examine the behaviour of concrete straps prestressed with GFRP bars subjected to axial tensile forces. Six straps were cast in the structures' laboratory at the University of Manitoba, of which, three were tested after 43 days of casting and the rest were constructed for future research to assess their durability.

The length of the strap between the anchors was 1500 mm and the length of the anchors was increased to 375 mm. The strap was pretensioned by two # 5 C-Bar stressed to 55% of their 5th percentile tensile strength, 440 MPa.

5.2.2. Preparation of Materials and Test Set-up

5.2.2.1.Casting of Anchors for the GFRP Bar

The bars supplied by the manufacturer came in 6 m lengths. Therefore; it was decided to cast two concrete straps in one length of the GFRP bar. The epoxying of

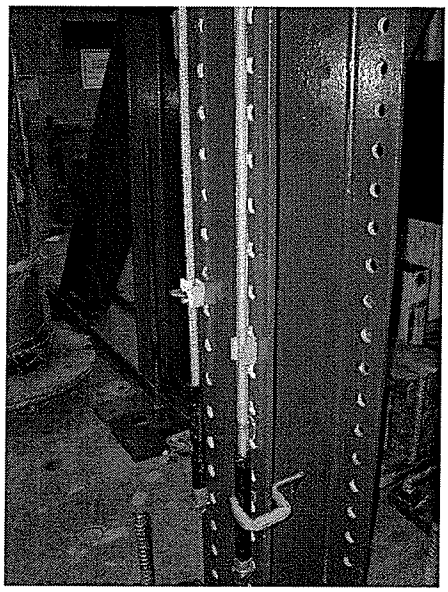

Figure 5.11
Epoxying the Steel Sleeves
as Anchors for the GFRP

the steel sleeves as anchors for the GFRP bar was done in a similar procedure as was done for the tension test specimens. Keeping the 6m long GFRP bars in an upright position required utmost caution to avoid damage by bending and twisting. Figure 5.11 shows the setup for attaching anchors to the GFRP bar. The GFRP bar was clamped at every 1.5 m interval to the steel column. Gauze bandages and U-shaped wooden pieces acted as cushions between the steel clamp and the column for added protection.

5.2.2.2.Developing and Testing of the Coupler

The anchor used for testing the GFRP bar in tension could not be used for stressing the bar for a period of time, because of the fear of crushing of the bars in the grips and ultimately failure of the bars without any sufficient prior notice. Therefore a coupler was used for prestressing, as shown in figure 5.12. The coupler was made of grade 300W steel. This method was better for one more reason, as it was easy to release the stress after the concrete has reached its desired compressive strength by cutting the steel tendon rather than cutting the GFRP strand.

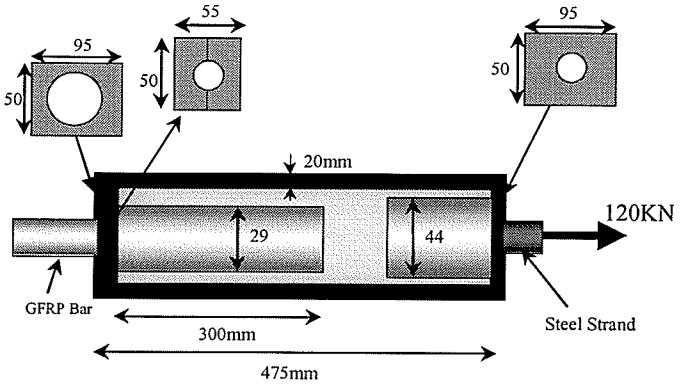

Figure 5.12
Coupler for Stressing the GFRP Bar

An analytical study was done on the coupler with the help of SAP 2000 program to check whether the coupler would sustain the stresses subjected to it. The strength of the coupler was confirmed by testing (Figure 5.13) under a tensile that was 150% of the required pretensioning force. A second pilot test was done to confirm the adequacy of the coupler to stress the GFRP bar without crushing it in the gripping zone (figure 5.14). The bar showed no sign of distress during this test.

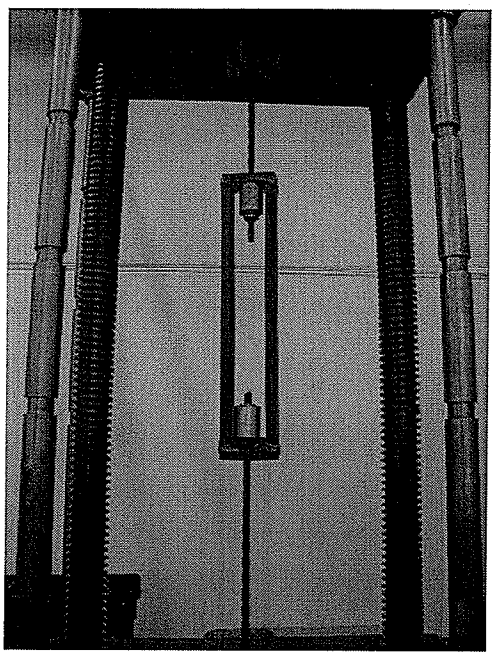

Figure 5.13
Testing of Coupler

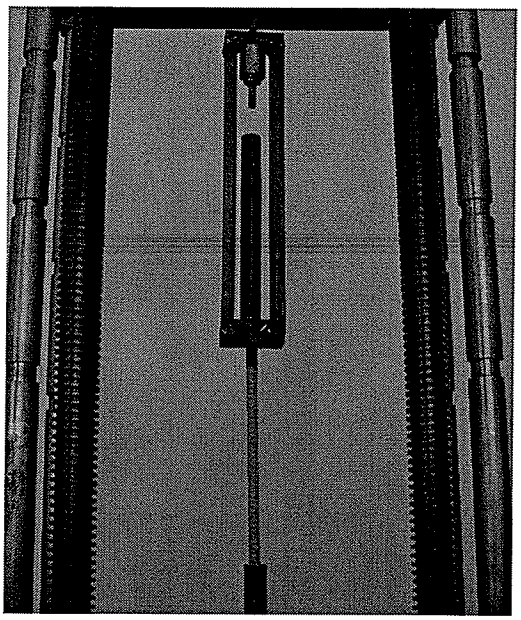

Figure 5.14
Stressing the GFRP Bar

5.2.2.3.Anchorage Zone – Design

In pretensioned concrete specimens, the prestressing force is introduced as a concentrated load, gradually over the transfer length. The compressive stress distribution in the concrete becomes constant after transfer zone that is roughly equal to the depth of the beam. The transverse tensile stresses that are developed during the stressing operation and are also known as Hoyer effect may lead to longitudinal cracking of the member if they exceed modulus of rupture of concrete. Typically, there are high bursting stresses along the axis of the load a short distance inside the end zone, and high spalling stresses set up at the loaded face (Collins and Mitchell, 1997).

To control the bursting and splitting stresses near the ends of the straps, the anchorage zone was more heavily reinforced at either end, which consisted of eight 12 mm diameter threaded steel rods and CC-0.125 wire mesh, which was an improvement over the previous test on reinforced concrete straps. The length of the anchorage zone was also increased from 300 to 375 mm.

5.2.3. Stressing the GFRP Bar

5.2.3.1.Instrumentation of the GFRP Bar

The GFRP tendons were instrumented with conventional strain gauges both in the longitudinal and transverse directions. Thermo-couples were also installed to see the influence of hydration temperature of concrete on the GFRP bar (Vogel H., 2002). The strain gauges were placed in such a way that, after being stressed, the strain gauge would be in the desired location i.e. one at the centre of the strap and others at 500 mm from the centre, either side.

5.2.3.2.Prestressing Setup

The prestressed concrete straps were manufactured in the prestressing bed shown in figure 5.15. The tendons were tensioned against bulkheads, which had a capacity of more than 300 kN. Two different types of bulkheads were used to facilitate construction of 3 sets of concrete straps at the same time. The GFRP bars were centred with the help of ends of the formwork, which had holes in them at the required height and width. Plastic chairs were not used to position the bars, thus, avoiding potential crack initiators.

Each sleeve of the GFRP bar was connected to the coupler and the coupler was connected to a 12.7 mm diameter seven-wire strand steel tendon as shown in figure 5.16. The steel tendon is connected to the bulkhead, which transfers the forces due to prestressing to the 1m thick strong floor. Figure 5.17 shows the jacking end of the setup, while figure 5.18 shows its dead end

The tensioning force in the GFRP tendons was controlled by calibrated hydraulic pressure gauge, strain gauges and also verified mechanically by measuring the elongation during the tensioning process using a tape measure.

The bars were stressed one at a time while adapting adequate safety measures. Because FRP tendons are brittle and may break suddenly during stressing, personnel operating the stressing devices were standing away from the set-up as well as had

safety glasses and safety hats to safeguard against the possible explosive release of energy stored in these tendons during stressing.

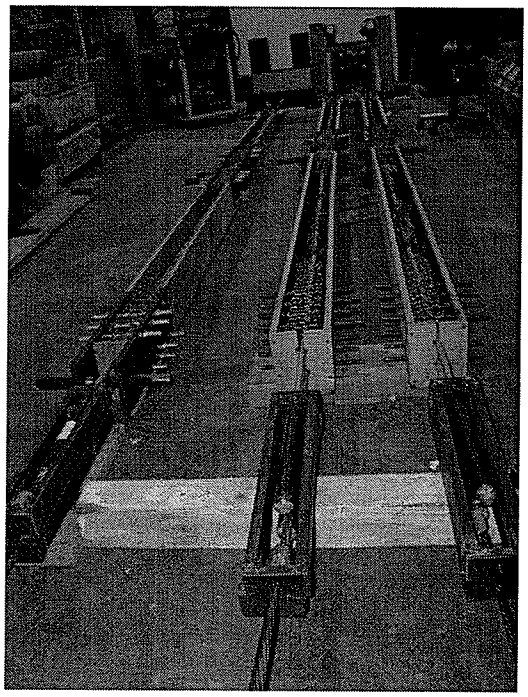

Figure 5.15
Prestressing Setup

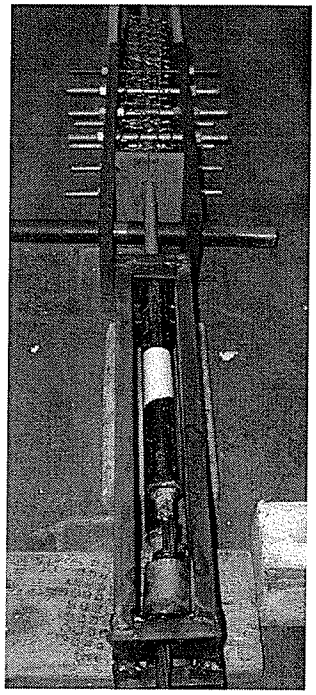

Figure 5.16
Pulling Mechanism

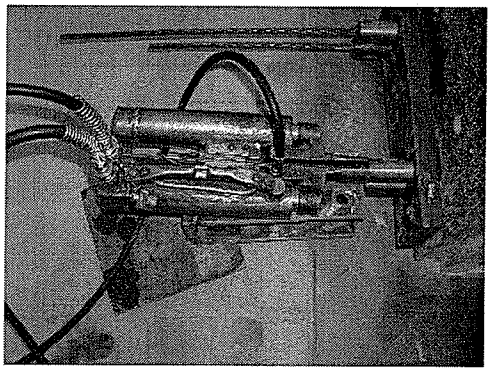

Figure 5.17
Jacking End

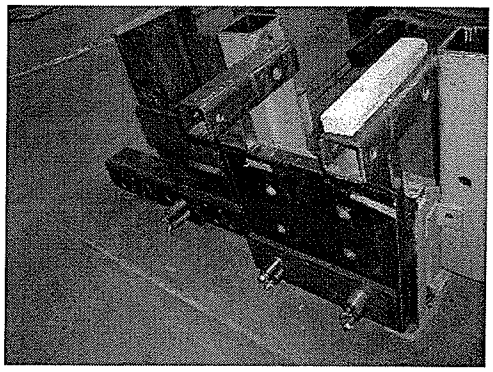

Figure 5.18
Dead End

The tensioning of the GFRP bar was done late in the afternoon so that, in the event of the failure of bar, there would not be many students or technicians around. Casting of the straps was done early on the next day and care was exercised during placement of concrete so that vibrations of tamping rods do not damage the tendons and attached instrumentation.

5.2.4. Concrete

40 MPa concrete was specified for construction of prestressed concrete straps. The mix design and mechanical properties of the concrete used in the straps are given in table 5.2.

Table 5.2: Concrete Mix Design and Properties

Component	Value
Cement	400 kg/m^3
Classified Sand	938 kg/m^3
Water	150 kg/m^3
10mm Coarse Aggregate	836 kg/m^3
WRDA	1 L
Air Entraining Agent	20 ml
Water Cement Ratio	0.371
Density of Concrete	2342 kg/m^3

5.2.4.1. Material Testing

Compressive strength and the modulus of elasticity of concrete mix were determined by means of standard tests for compressive strength in accordance with ASTM C 39 and ASTM C 469. Additionally, splitting tensile strength of cylindrical concrete specimens was also determined following ASTM C 496. These tests were done prior to releasing the stress, after 14 days and before testing the PC straps in axial tension, the results of these tests are shown in Table 5.3. The concrete cylinders tested for compression were instrumented with a strain gauge longitudinally and were monitored with the aid of a strain indicator as shown in figure 5.19.

Table 5.3: Mechanical Properties of Concrete

No. of Days after Casting	Compressive Strength (MPa)	Modulus of Elasticity (MPa)	Direct Cracking Strength (MPa)
6	34.56	25934	1.55
14	38.09	28916	1.78
43	41.26	30529	2.09

Figure 5.19
Test on Concrete

5.2.5. Strain Monitoring of the GFRP Bar

Strains were continuously monitored from the time the bars were stressed to the time the stress was released in the bars after the concrete had set. This was achieved by connecting the strain gauges to the data acquisition. Few of the strain gauges were also connected to the strain indicator to check the uniformity of the strains in the bar as well as to conform the strain results displayed by the data acquisition.

The frequency of recording the data was a reading every two seconds until the time concrete was poured in the formwork. After that, the frequency was reduced to a reading every five minutes to limit the number of data points. The strain was recorded for 8 days.

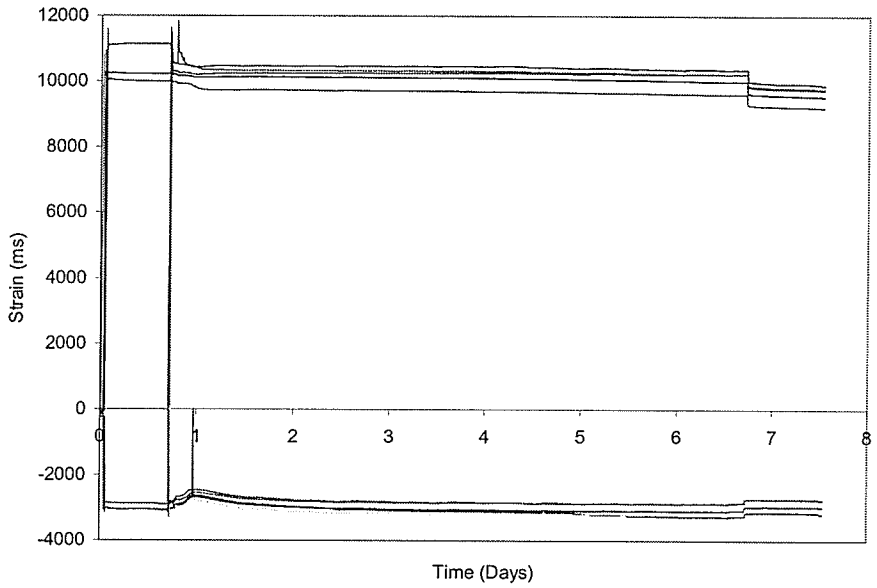

Figure 5.20
Strain Monitoring

Figure 5.20 shows the change of the strain with time before and after casting. Longitudinal strains are shown in the positive quadrant and the transverse strains are shown in the negative quadrant owing to Poisson's effect. Any point on the graph would yield a Poisson's ratio of about 0.28 for the considered bar, thus, validating the initial test result described in section 3.

The maximum permissible stresses in GFRP tendons at jacking and transfer for concrete beams and slabs based on CHBDC (2000) are 0.55 f_{pu} and 0.48 f_{pu}, respectively. The permissible stress levels were kept low so that the creep and relaxation and the corresponding prestress losses also remain small. The high stresses in FRP during prestressing in combination with higher transverse coefficient of thermal expansion may cause cracking due to Hoyer effect.

GFRP has a very low modulus of elasticity than that of steel and therefore the prestress losses in components with FRP tendons are expected to be smaller than of those in components with steel tendons.

The strains at all the critical junctures in the history of the bar, from the time of jacking till the time of the last reading, were converted into their respective stresses with the help of stress-strain relationship derived from the previous tests and are

shown in table 5.4. It was found that the loss in prestress was about 14%, which included relaxation losses and other time dependent losses.

As it can be seen in table 5.4, the stress in strap B during jacking was comparable to those in the tendons of other straps; however the tendons of this strap lost more stress during concreting, possibly due to vibration while pouring concrete. It will be later seen that, the cracking load for strap B was the smallest of the three straps.

Table 5.4: Stresses at Different Stages of the GFRP tendons

		Stress / Ultimate strength of the tendon					
		Jacking stress	After jack release	After concreting	Just prior to stress release	After stress release	Last reading
Time/Date		-	5:31PM 20 AUG	7:30PM 21 AUG	1:45PM 27 AUG	2:05 PM 27 AU	2:05 PM 28 AUG
Strap A	T	**0.547**	**0.527**	**0.517**	**0.505**	**0.488**	**0.482**
	B	**0.554**	**0.525**	**0.518**	**0.515**	**0.494**	**0.493**
Strap B	T	**0.553**	**0.520**	**0.503**	**0.493**	**0.485**	**0.470**
	B	**0.559**	**0.536**	**0.500**	**0.502**	**0.486**	**0.482**
Strap C	T	**0.557**	**0.523**	**0.517**	**0.511**	**0.493**	**0.487**
	B	**0.554**	**0.517**	**0.513**	**0.509**	**0.495**	**0.489**

T = Top Bar

B = Bottom Bar

5.2.6. Releasing the stress

As mentioned previously, the use of couplers made it easy for releasing the stress. The stress was released by cutting the steel strands by means of a torch as shown in figure 5.21. Proper safety measures were implemented when releasing the stress in the straps.

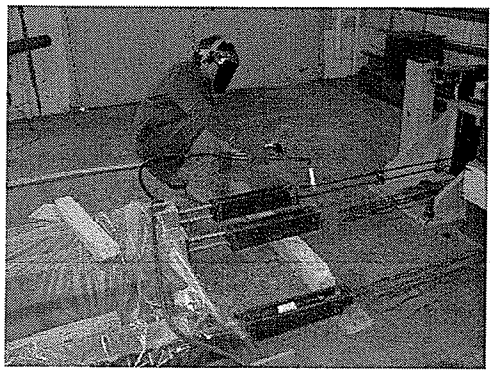

Figure 5.21
Releasing the Stress

5.2.7. Instrumentation of the prestressed concrete strap

Midway between their ends, the prestressed concrete straps were instrumented with four PI gauges placed on each of their four faces. LVDTs were mounted at each end to measure the slip between the concrete and the anchorage zone (Figure 5.22). Additionally, a linear motion transducer (LMT) was installed to measure the elongation of the strap. The loading and load measuring mechanism was exactly similar to those used for RC straps.

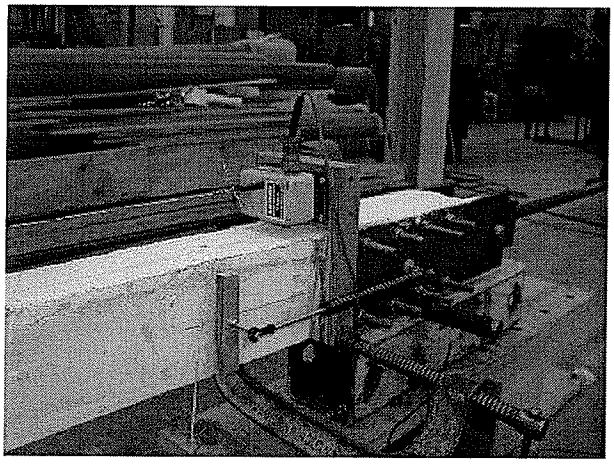

Figure 5.22
PC Strap Instrumentation

5.2.8. Description of Testing

Each strap was first subjected to 50 cycles of gradually increasing load of 50 kN, and then tested until failure by applying a steadily increasing load and observing the crack patterns at each load step. The load was increased until 250 kN, at this level the pin which connected the strap to the pulling mechanism started to yield, therefore, the test had to be terminated. The main objective of the test was to determine the cracking load and therefore this flaw of the test set-up did not constitute a major problem.

5.2.9. Observed Cracking Behaviour During Testing

The PC straps did not crack during the cyclic testing under 50 kN force, but during the ultimate loading, the PC straps exhibited a characteristics sequence and pattern of cracking. A typical crack pattern for one of the straps is shown in figure 5.23. The cracking pattern for the PC straps was different from that of the RC straps in the following manner-

- The number of cracks were smaller and the spacing of the cracks greater than those of RC straps.
- There were cracks in the longitudinal direction of the strap, unlike RC straps, which had cracks only in the transverse direction. This was indicative of bond failure of GFRP bar

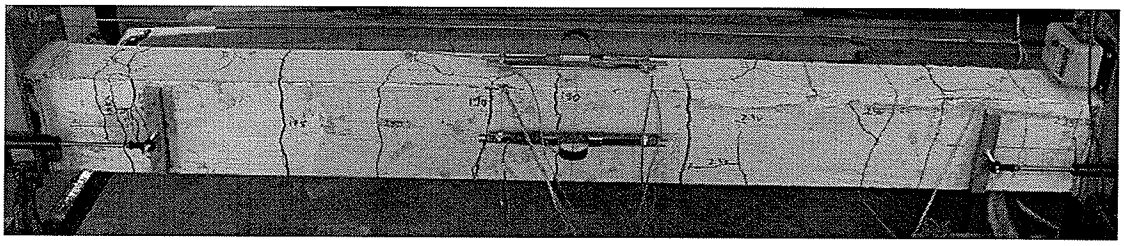

Figure 5.23
Crack Pattern – PC Strap

5.2.10. Load-Strain Results

After the fatigue study, the strap was taken to a load of 250 kN. The plot for the three straps is shown in figure 5.24. As can be seen from the graphs, the cracking

load varied from 155 to 180 kN, depending upon the prestressing force after stress release. The smallest cracking resistance was for strap B. The three graphs are also compared with their respective analytical graphs as described in chapter 4. The only variable in the three straps was the prestressing force, which was estimated on the basis of the last reading observed. After cracking there is a sudden drop in the stiffness of the member as, the concrete becomes ineffective in sharing the stress and the FRP takes over. The rising curve of the load – strain plot, after an initial plateau, shows the effect of tension stiffening.

Figure 5.25 shows the slip between the anchorage and the concrete for Strap I. The elongation shown in the graph is subsequent to the cracking load level of the concrete and there were cracks in between the ends of the LVDT, suggesting that there wasn't any slip. It was noted that for all the straps, the jacking end had far more cracks than the dead end.

Figure 5.26 shows the elongation measured by the LMT with respect to the applied load for the three straps. Although, the cracking loads were different for the three straps, the cracking pattern as well as the width of the cracks was similar. As mentioned earlier, strap B had far more cracks than straps A and C, but the width of these cracks were smaller.

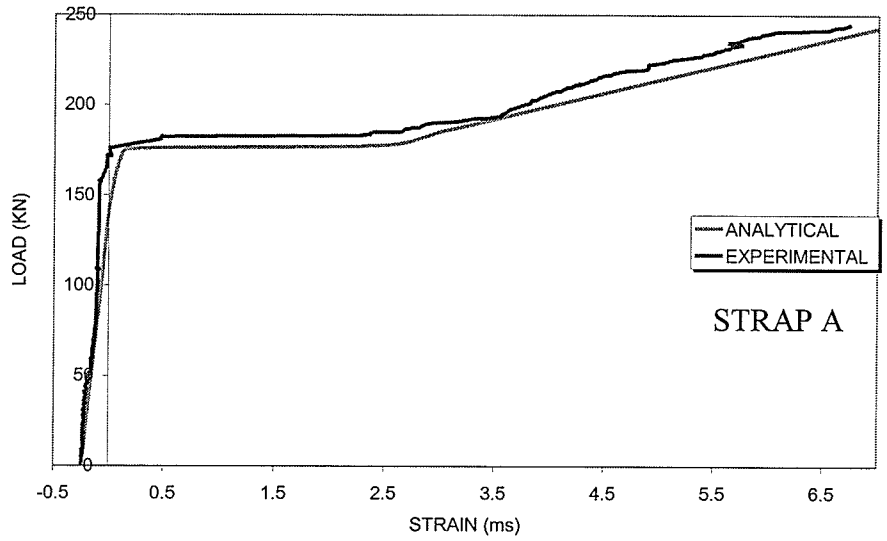

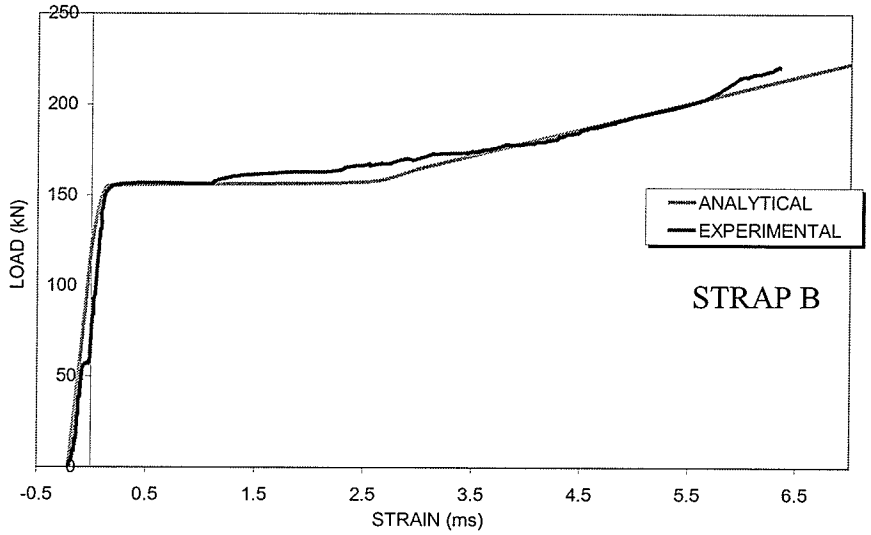

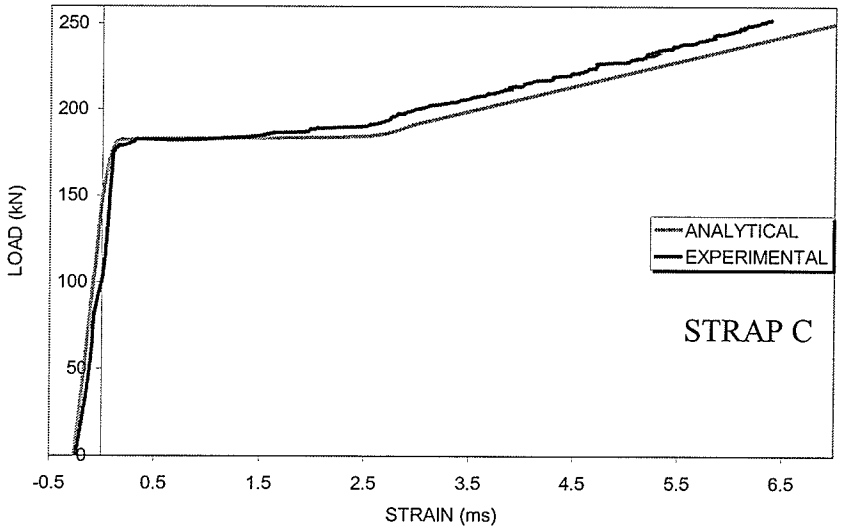

Figure 5.24
Static Loading – PC Straps

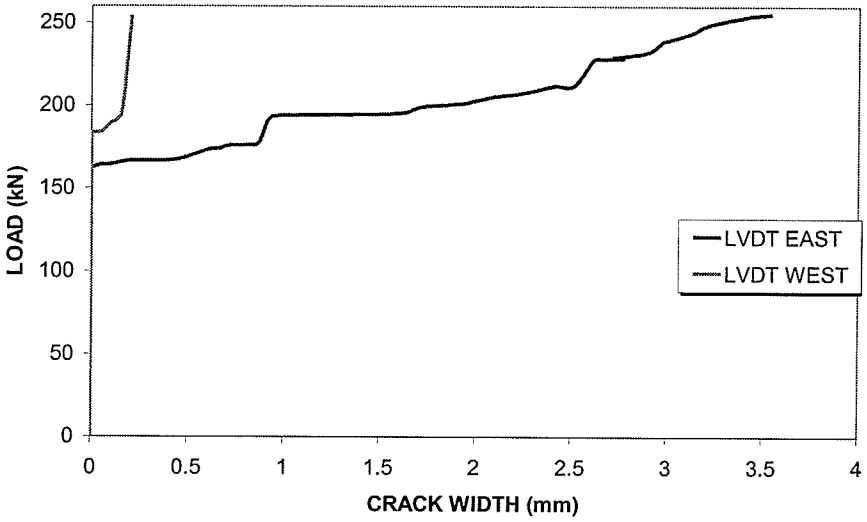

Figure 5.25
Slip between Anchorage and Concrete

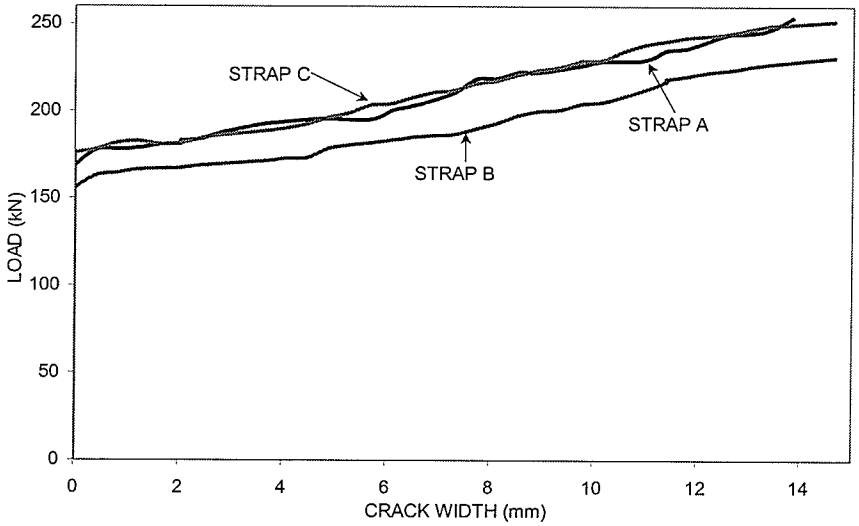

Figure 5.26
Crack Width Propagation

5.2.11. Conclusions

The tensile axial behaviour of un-cracked PC strap is compared to those of RC strap and steel strap in figure 5.27. It was confirmed that the PC strap would easily sustain the required tensile force of 132 kN. Further, the axial stiffness of PC strap is significantly larger than that of the steel strap.

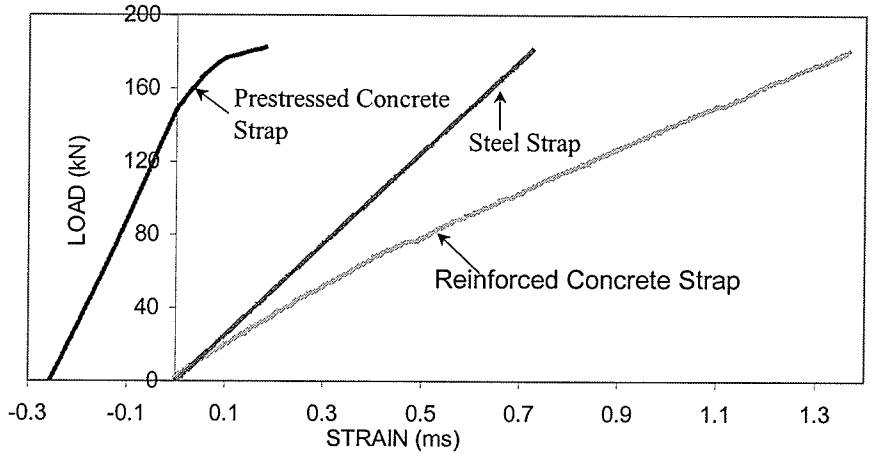

Figure 5.27
Comparative Axial Behaviour

5.3. Straps for the Deck Slab

Four PC straps were constructed for the transverse confinement of a full-scale partial model of a steel free deck slab. The casting of these straps can be seen figure 5.28. The length of the strap was 3 m of which 0.5 m at either end was the transfer length.

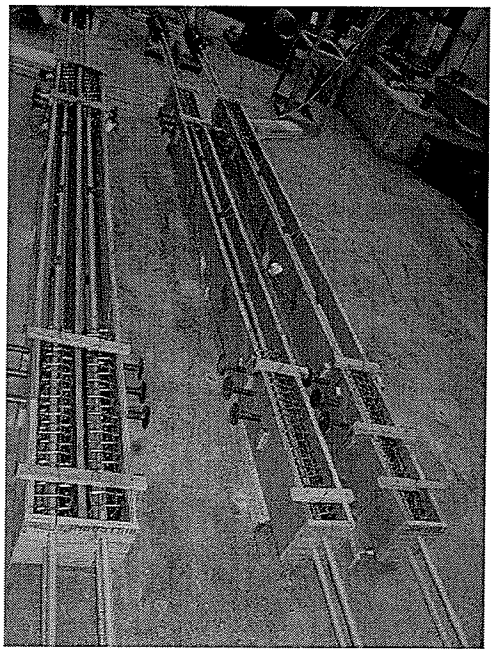

Figure 5.28
Straps For the Bridge Deck

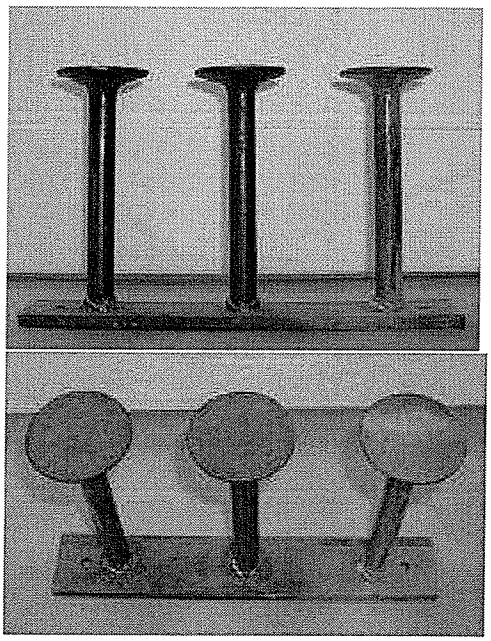

Figure 5.29
StudRail

The connection of the strap to the deck slab was achieved by using STUDRAILS™, in which the rail consisted of 3 studs at either end as shown in the figure 5.29.

Again, the strains of the PC straps were continuously monitored from the time the bars were stressed to the time the stress was released in the bars after the concrete had set. While stressing the GFRP strand for one of the straps, the steel sleeve started to slip, with a loss of strain in the GFRP bar. It was decided to postpone the stressing until the following day, just before the time concreting was scheduled. This remaining bar was stressed on the day of the concreting without any problems; the strains were followed during the entire operation of concreting to check the possible slippage, if any.

5.3.1. Concrete Mix Design and Properties

The mix design and mechanical properties of the concrete used in the straps are given in table 5.5.

Table 5.5: Concrete Mix Design and Properties

Component	Value
Type 30 Cement	500 kg/m^3
Water	200 kg/m^3
Coarse Aggregate	1034 kg/m^3
Fine Aggregate	620 kg/m^3
Properties	
Slump	95 mm
Density	2417 kg/m^3

The stress in the straps was released on the 12th day after adequate compressive strength of concrete was achieved according to testing the concrete cylinders in compression. The mechanical properties of the concrete used in the straps

are given in table 5.6. The stress was released by cutting the steel strands with a torch. After cutting the steel strands for one of the straps, the strap failed with a loud noise by concrete spalling off and exposing the GFRP bars. On investigation, it was found that the possible reason for the failure of the strap was either warping of the plywood that was used for casting the strap or translation of the formwork sideways due to the use of vibrator during concreting. Therefore, when the stress was released, it created an unbalanced transverse force causing the strap to split longitudinally as can be seen in figure 5.30.

Table 5.6: Mechanical Properties of Concrete

No. of Days after Casting	Compressive strength (MPa)	Modulus of Elasticity (MPa)	Direct cracking strength (MPa)
6	21.89	20963.44	-
12	30.59	25994.52	1.87
28	36.64	-	2.28
70	45.82	-	-

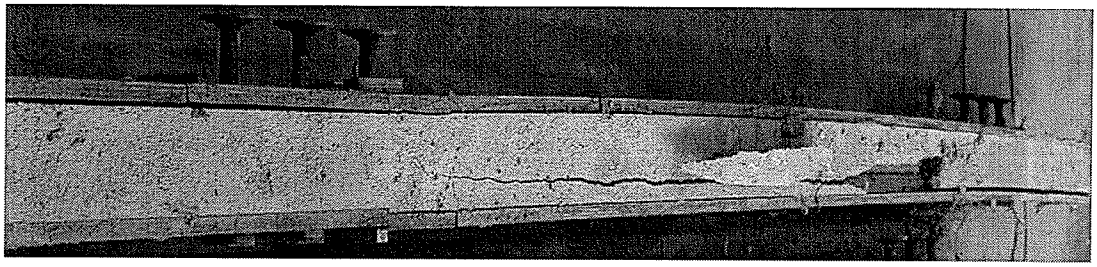

Figure 5.30
Failure of Strap

It was decided to construct a fibre reinforced steel-free deck slab laterally confined by three prestressed concrete straps spaced 1000 mm apart.

Chapter 6

ANALYTICAL MODEL FOR STEEL FREE DECK SLAB WITH PRESTRESSED CONCRETE STRAPS

6.1. Introduction

Prior to designing, constructing and testing the steel free deck slab with prestressed concrete straps as transverse confinement, an analytical study was carried out using the PUNCH program based on a rational developed by Mufti and Newhook (1998).

The PUNCH program was developed to predict the behaviour of laterally restrained concrete slab-on-girder bridge decks under the wheel loads of heavy trucks. The program requires input of specific geometric and material properties and will produce load-deflection data for the deck as well as predict the ultimate failure load of the deck slab in punching.

Under an increasing concentrated wheel load, a concrete slab on girder bridge deck will eventually form a crack pattern, as shown in figure 6.1. This divides the area of the deck close to the wheel load into a series of concrete wedges bounded by the crack pattern. Under load, these wedges will rotate to an equilibrium position based on the geometry of the system and the amount of lateral restraint provided. An idealisation of this rotation is shown in figure 6.2. Using the equations of equilibrium, a series of equations can be developed for the various forces acting on the wedges. Further expressions can be developed to quantify the amount of lateral restraint as well as the degree of confinement provided to the concrete at the tip of the wedges around the wheel load. It is noted that the concrete in this region is in a state of three-dimensional compression and it is the failure of the concrete in this region that leads to the ultimate failure of the slab by punching.

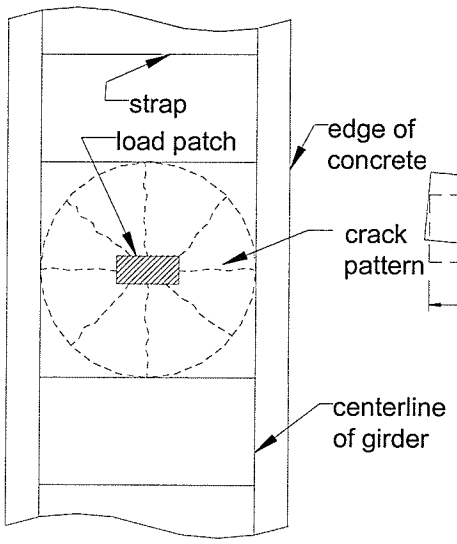

Figure 6.1
Crack Pattern in Concrete Deck
under Concentrated Load

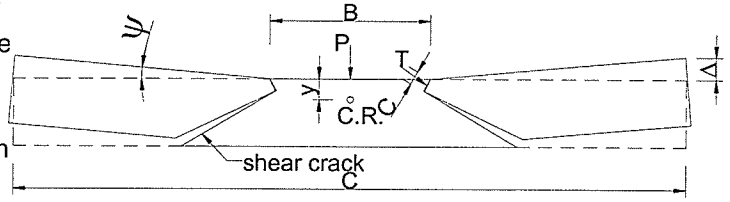

Figure 6.2
Rotation of Wedges
under Loading

Finally, the failure conditions are applied to the model to create a complete algorithm for predicting the behaviour of bridge decks. The equilibrium condition is then compared to two failure criteria: crushing of the concrete around the loaded area or failure of the straps either by yielding (steel straps) or cracking (prestressed concrete strap) which will initiate subsequent crushing of the concrete.

A complete description of the rational model can be found in Newhook (1997).

6.2. Model Parameters

A typical steel-free bridge deck with prestressed concrete strap as transverse confinement is shown in figure 6.3. From this figure, the key modelling parameters are:

S_g Spacing of girders

S_l Length of strap

A Area of tire print of dimension b x w

S_s Spacing of straps

d	Depth of concrete
E	Modulus of elasticity of strap material
f'_c	Compressive strength of concrete in bridge deck
β_1	Rectangular stress block parameter
K	Transverse restraint stiffness
k	Concrete confinement constant
ε_y	Yield strain of steel strap / Cracking strain of PC strap
B	Diameter of equivalent circle for loaded area
D	longitudinal distance from wheel load to nearest strap
A_s	Cross-sectional area of strap

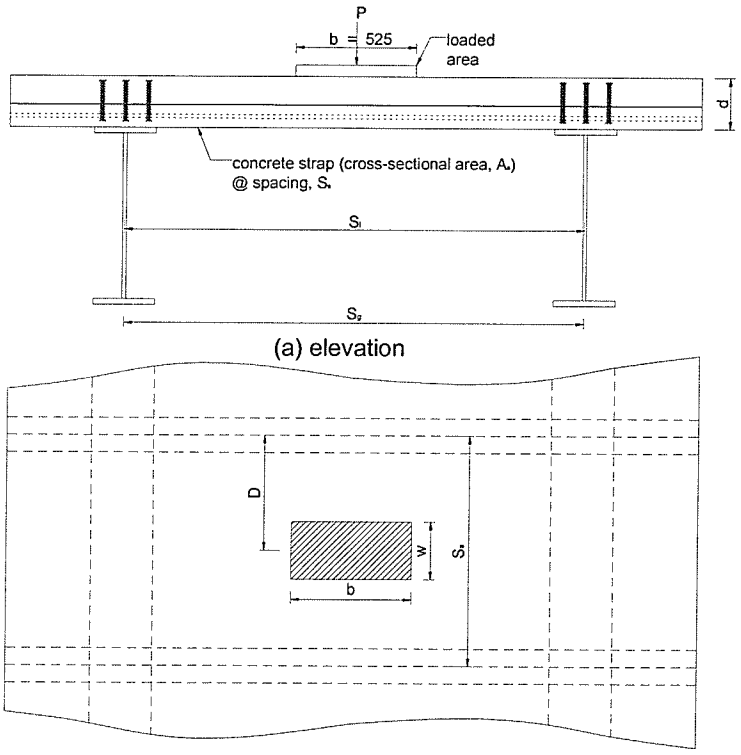

Figure 6.3
Steel Free Bridge

For steel free deck slab laterally restrained with prestressed concrete straps, the following parameters need further refinement because of their different behaviour as compared to steel straps.

6.3. Modulus of Elasticity of Strap

The load - strain curve of one of the strap, prior to its cracking is drawn in figure 6.4; the slope of this curve is determined as shown in the graph. Based on this equation the modulus of elasticity for a member exhibiting a linear relationship is determined by Hooke's law:

$$\sigma = E\varepsilon \tag{1}$$

$$\frac{F}{A} = E\varepsilon$$

or

$$E = \left(\frac{F}{\varepsilon}\right)\left(\frac{1}{A}\right) \tag{2}$$

where,

σ = Stress in the strap

ε = Strain in strap

F = Applied Load on the strap

E = Modulus of elasticity of the strap material

A = The area of cross-section of the strap

As calculated, F/ε, the slope of the curve is equal to 5.8 x 10^8 N, and the cross-

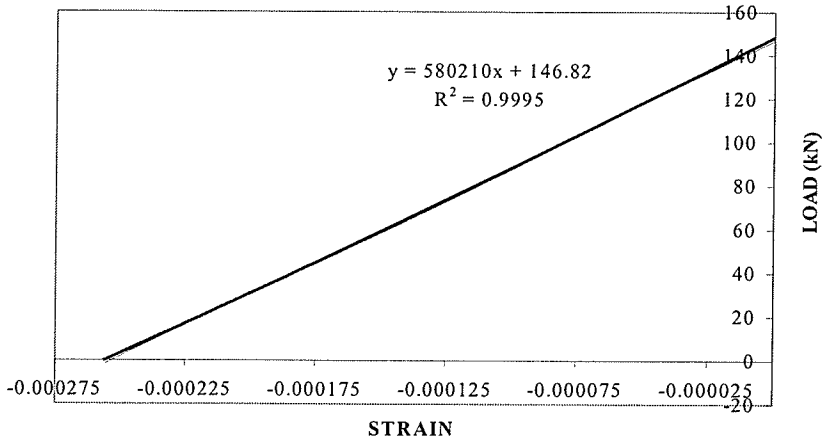

Figure 6.4
Slope of the Load Strain Curve

sectional area of the transformed section of the PC strap is equal to 15182 mm^2. Using the above values yields the modulus of elasticity as 38203.13 MPa.

6.2.1. Transverse Restraint Stiffness

The actual transverse restraint stiffness includes both the effects of the restraint from the straps as well as the restraint from the girders, the latter is however generally ignored. The restraint stiffness, k, contributed by only the straps is calculated as follows;

$$K = \frac{EA}{0.5S_l S_s} \tag{3}$$

$$K = \frac{38203.13x15182}{0.5x2000x1000}$$

$$K = 580MPa$$

6.2.2. Cracking Strain of Strap

There is a substantial loss in stiffness of the prestressed concrete strap, once the concrete cracks, therefore the cracking strain of the strap is considered as the limiting value and not the rupture strain of the GFRP, which is calculated to be about 0.0004. This value varies depending upon the initial prestressing force in the strap. It will increase, if the initial prestressing force is higher and it will decrease if the prestressing force is lesser.

6.3. Bridge Deck Model for Analysis

The bridge deck shown in figure 6.3 was analysed using the PUNCH program (Mufti and Newhook, 1998). The following material properties were used in the analysis:

Concrete compressive strength, $f'_c = 35$ MPa

Strap strain at failure, which corresponds to its cracking strain, $\varepsilon_{strap} = 0.0004$

Concrete constant used for confinement, $k = 10$

Rectangular stress block parameter, $\beta_1 = 0.81$

Modulus of elasticity of strap material, E = 38203.13 MPa.

The area of the load patch, Δ, is calculated to be 125,000 mm^2 and the diameter of equivalent circle for load patch, B, is calculated to be 477 mm. The input data for the Punch program are tabulated in table 6.1.

Table 6.1: Input Data for PUNCH

S_g	B	f'_c	K	D	d	β_1	k	Δ	ε_{strap}
2000	477	35	580	0	175	0.81	10	125000	0.0004

The output file provides the failure load corresponding to the cracking strain of the prestressed concrete strap. The output file is shown in figure 6.5

UNITS – METRIC - kN, mm, Second
Clear Span Between Girders = 2000.00
Diameter of Equivalent Circle for Load = 477.000
Maximum Compressive Stress of Concrete = 35.0000
Elastic Axial Stiffness of Strap = 581.000
Strap to Load Spacing = 0.000000
Depth Of Slab = 175.000
Beta to Define Rectangular Stress Block = 0.810000
Concrete Constant used for confinement = 10.0000
Area of Load Patch = 125000.
Yield (Cracking) strain = 0.400000E-03

DELTA	**ALPHA**	**P**	**STRN**
0.00	0.00	0.	0.00000
0.50	19.71	70.	0.00009
1.00	18.74	135.	0.00017
1.50	17.99	197.	0.00025
2.00	17.38	255.	0.00032
2.50	**16.86**	**310.**	**0.00040**
3.00	16.80	308.	0.00047

******* **Punch Load-Cracking Strain in Strap** *******

Figure 6.5
Output File – Punch Program

PUNCH load corresponding to the cracking strain in strap indicates that the cracking of the prestressed concrete strap initiates punching failure, as the strap is unable to sustain very high axial loads due to its increased stiffness as compared to a conventional steel strap.

6.4. Rationale for Constructing and Testing Deck Slab with PC Straps

The OHBDC (1979), and recently CHBDC (2000), permit a reinforced concrete deck slab with a minimum thickness h_{slab}, of 175 mm. The largest girder spacing is given as 15 h_{slab}, which is for 175mm deep slab equal to 2.625 m. It is assumed that 30 MPa concrete is used, and the bottom transverse reinforcement is the smallest permitted by the codes, i.e. 0.3 % of the area of concrete. The charts given in the various editions of the OHBDC give the static failure load of this slab to be about 750 kN.

By contrast, the theoretical failure load of an FRC slab with pretensioned concrete straps is typically about 300 kN, the failure being caused by the inadequacy of the straps to sustain very large axial loads. It is argued in the following that notwithstanding its relatively low failure load, the proposed slab has adequate strength.

From the Calibration Report (CHBDC, 2000), it can be calculated that the annual maximum axle loads in Ontario, Alberta, Saskatchewan, Quebec and New Brunswick are 314, 150, 134, 211 and 159 kN, respectively. As noted by Mufti et al. (2002), the maximum lifetime axle load anywhere in Canada is expected to be 345 kN. The maximum axle load observed in Japan is 32 t, or 313 kN (Matsui et al., 2001). To be conservative and following the practice of BC Ministry of Forests, it is assumed that the wheel loads on an axle are distributed in the 60:40 ratio. Thus, the maximum wheel load expected during the lifetime of a bridge in Canada is 207 kN (= 0.6×345). It is interesting to note that corresponding factored wheel load of the CL-625 Truck (CHBDC, 2000), including a dynamic load allowance of 0.4, is calculated to be 208 kN.

Since slabs designed by the OHBDC/CHBDC empirical method are not known to fail in fatigue, it is assumed that the above 'weakest' deck slab would also not fail in fatigue. It is further assumed that if the static failure load of a deck slab is at least 750 kN, the slab is not likely to fail in fatigue during its lifetime. This presumption is valid for only those slabs, which fail in punching shear under the monotonically increasing, or static load, and in which the lateral restraint does not yield/fail prior to the punching shear failure of the slab. It is also important to note that during its lifetime, a deck slab is not expected to be subjected to a wheel load heavier than 207 kN. As noted in the section 2.3, a wheel load of about 400 kN induces a tensile force of only 50 kN in a typical strap.

Consider a deck slab confined by straps of metal "X", which has the same modulus of elasticity as that of steel, but its yield strength is much smaller. Now subject this slab to lifetime of wheel loads. As long as the straps themselves do not fail in fatigue, nor yield under the maximum lifetime wheel load (i.e. 207 kN), the deck slab would have the same fatigue resistance as that of slab with steel straps. Although the hypothetical metal straps do not permit the slab to develop its full static strength, the arching action is maintained under loads smaller than 207 kN. In this case, there is no reason to worry about the 'full static strength of the slab', which is never utilised anyway.

After due consideration, we can conclude that as long as the prestressed concrete straps remain elastic under wheel loads of up to 207 kN, the concept of using PC straps for transverse confinement is feasible. Therefore it was decided to design, construct and test the proposed concept by means of a full-scale partial model.

Chapter 7

EXPERIMENTAL INVESTIGATION OF BRIDGE DECK BEHAVIOR

7.1. General

The prototype bridge form chosen for experimental investigation was a short span highway bridge with longitudinal steel girders made composite with the deck slab. The experimental section consisted of a typical two-girder interior longitudinal slice of the prototype structure. The 9000 mm long girders (W 760 X 196) were spaced at 2000 mm and were connected at each end by cross-frames. Three prestressed concrete straps were placed on top of the girders between the steel studs at a spacing of 1000 mm, as shown in figure 7.1. The fibre reinforced concrete deck was 175 mm thick with 50 mm haunches over each girder. Typical plan views and cross-sections are shown in figure 7.2 and 7.3, respectively.

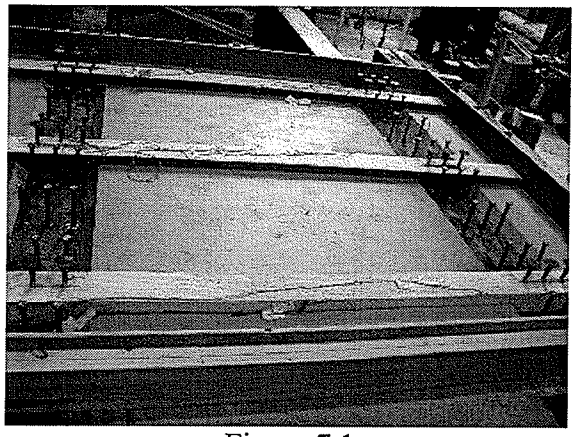

Figure 7.1
Placement of the PC Straps

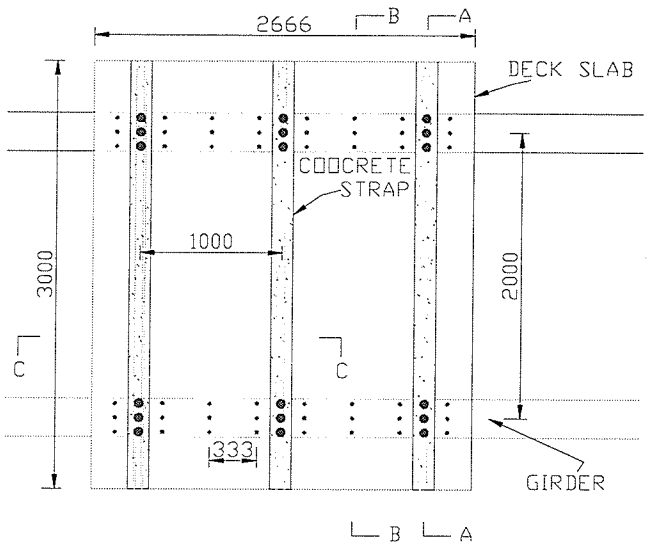

Figure 7.2
Partial Plan of the Deck Slab

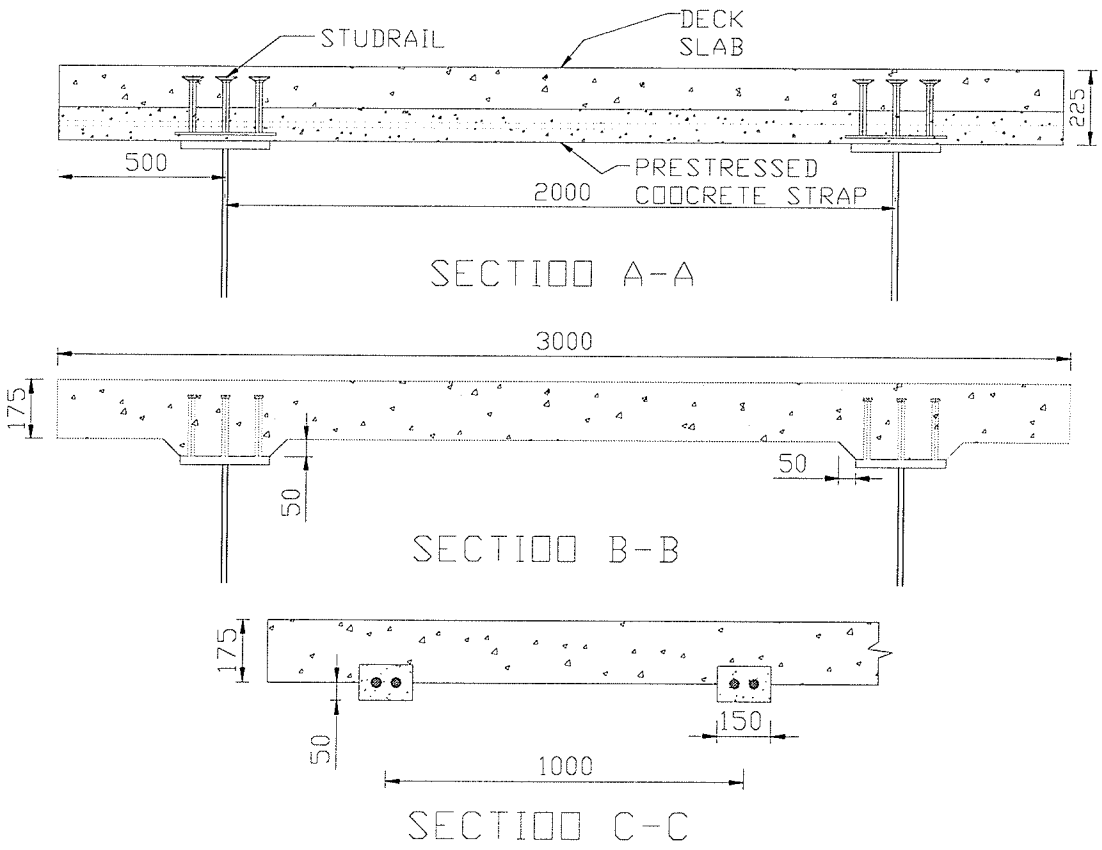

Figure 7.3
Sectional Elevations of the Deck Slab

7.2. Design of Full-scale FRC Bridge

7.2.1. Steel Girders

The slab test loadings were the governing design load for the steel girders of the test bridge. Stresses were calculated to ensure that the maximum stress in the W 760 X 196 girder would be less than the steel yield stress. Shear connection between the steel and concrete was ensured through the use of stud-type steel shear connectors. The studs were 20 mm in diameter and were welded in groups of three to the top flange of the girders at 333 mm centres along their length.

7.2.2. Prestressed Concrete Strap – Deck Slab Connections

The prestressed concrete straps were placed directly on the girders, within the spaces between rows of shear connectors. The formwork of the slab was interrupted by the straps as can be seen in figure 7.4. It can also be seen in figure 7.4, that the straps are partially embedded in the slab, with the depth of embedment varying along the length of span to accommodate the requirement for camber. An advantage of this scheme lies in the elimination of the difficulty in removing the formwork over the steel straps.

Figure 7.4
Bottom View of Deck Slab

7.2.3. Description of FRC

Conventionally used in the steel free deck slabs, 35 MPa concrete was specified for construction of the cast-in-place deck slab for the test bridge. The specifications given to the concrete supplier are given in table 7.1

Table 7.1: Concrete Specifications

SPECIFICATIONS	VALUE OBTAINED
The quantity of concrete required	2 m^3
Type of cement	Type 10
The required slump at the point of discharge	75-85 mm
The nominal maximum size of coarse aggregate	20 mm
The air content for air entrained	6%
The mix proportions or Class of exposure	F2
Temperature of concrete	10-15° C
14 day compressive strength	35 MPa
Superplasticizer	1 L/m^3

The utilisation of fibres usually requires slight mix design modifications in order to offset any reduction in slump that may occur. An increase in the total cementitious content, a higher fine to coarse aggregate ratio and the use of superplasticizer will restore the required workability to fibre reinforced concrete. FORTA FERRO^{TM} fibres were added to the ready mixed concrete in the ratio of 0.4 % by volume. These fibres were monofilament and fibrillated fibres and were 54 mm long.

7.2.4. Material Testing

As a check of the concrete quality as supplied, limited material tests for workability and strength were performed on the concrete as delivered by the local ready-mix concrete supplier- Lafarge. The concrete slump was measured and

cylinders were prepared for compressive and tensile strengths. After the addition of superplasticizer the slump test was repeated and then the polypropylene fibres were added. The workability of the FRC was established by a test method that determines the time required for fibre reinforced concrete to flow through an inverted slump cone under internal vibration ASTM C 995-94. Compressive strength and the modulus of elasticity of plain concrete mix and the fibrous concrete mix were determined by means of standard tests for compressive strength as per ASTM C 39 and ASTM C 469. Additionally, splitting tensile strength of cylindrical concrete specimens was also determined according to ASTM C 496.

7.2.5. Cross Bracing

Cross frames were provided at the ends of the 9000 mm long girders, as can be seen in figure 7.5. These diaphragms were needed to provide stability to the steel girder system during erection and to stabilize the slender webs of the steel girders at the supports.

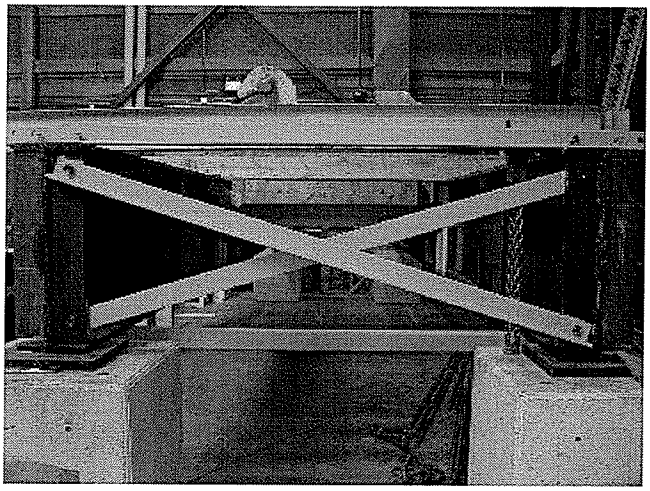

Figure 7.5
Cross-Bracing

7.2.6. Summary of Deck Casting

A description of the construction of the fibrous concrete slab in the formwork atop the steel framework of longitudinal girders and the prestressed concrete straps is provided below.

A 2 m^3 normal strength concrete batch mixed to specifications of Table 7.2, was delivered to the heavy structures' laboratory in a rotary drum concrete mixing truck.

Table 7.2: Mix Design for Concrete Delivered April 12, 2002

Mix code - GG35A61	Kg/m^3
Cement (type10)	304
Class C Fly Ash	76
Concrete Sand	794
20mm Stone	960
Water	148
Water reducer (322N)	1.2
Air Content (%)	5% - 8%

After testing the plain concrete for the slump as per ASTM C 143 and measuring the density, superplasticizer was added to the concrete. Two litres of superplasticizer were added to the concrete and the slump was measured again.

Polypropylene fibres were then added to the mix, directly to the drum while it was mixing at full mixing speed and care was taken to ensure large clumps did not go into the hopper. A total of 7.28 kg of fibre was added; i.e. 0.4% by volume of concrete. Once the fibres were added, the drum was stopped and rolled back to clean the fibres that were on the back fins and then mixing was resumed for 5 additional minutes at full mixing speed of 13 rev/min.

The drum had a capacity of 5 m^3 and was approximately half full before the addition of fibres and superplasticizer. Previous experiences of other researchers with fibre reinforced concrete suggested that the degree of difficulty in mixing fibres uniformly with concrete increases with the volume of the batch with respect to the size of the mixer. For example, a particular fibre volume can be mixed easily if the

mixer is only partially full but can be very difficult to mix if the mixer is at full capacity (Thorburn, 1996).

The uniformity of dispersion of the fibres in the concrete is confirmed visually and the measure of consistency and workability of fibre reinforced concrete is determined by measuring the time of flow of FRC through an inverted slump cone. This method is a better indicator than slump of the appropriate level of workability for FRC placed by vibration because such concrete can exhibit very low slump due to the presence of fibres and still be easily consolidated. It was the very first time that this test was done in the laboratory, therefore requiring a new set of apparatus. High

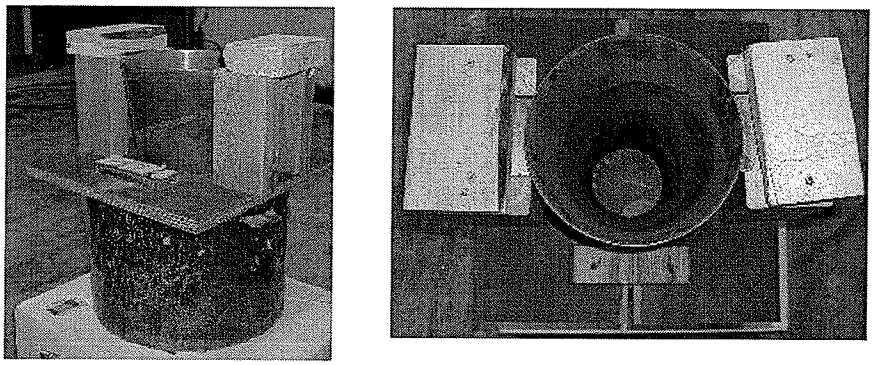

Figure 7.6
Time of Flow Apparatus

cost of a new set prompted us to build our own apparatus (Figure 7.6) thus, saving about $1000. As can be seen in the photograph, the materials used in building the apparatus were of no practical use in the laboratory.

The following information was gathered from the above-mentioned tests for both plain concrete as well as fibre reinforced concrete.

Type of Concrete	Slump	Density	Time of Flow
Plain Concrete	85mm	2390 kg/m^3	-
Fibre Reinforced Concrete	190mm (after adding superplasticizer)	2452 kg/m^3	12 sec

A 0.573 m^3 bucket was used to move the concrete from the drum to the slab formwork. A flexible shaft vibrator was used internally to consolidate the concrete in the deck form. While the truck was not discharging, the drum mixed very slowly because additional mixing would result in an increase in fibrillation, thus decreasing the workability. The deck was later finished manually and floated. Placing of the deck took approximately 2 hours. A plastic sheet covered the deck for curing for 7 days.

7.3. Description of Experimental Program

7.3.1. Description of Testing

To understand the fatigue behaviour of the steel free deck slab laterally confined by prestressed concrete straps, dynamic tests were conducted at two load levels. The experimental program was carried out in the Heavy Structures Laboratory at the University of Manitoba. The fatigue investigation on this deck was performed at load levels of 15 tonne (150 kN) and 21 tonne (208 kN). The loads were applied through a hydraulic actuator reacting against a steel-loading frame, which was attached to the structural floor of the laboratory. The load cell with a 1000 kN capacity was controlled by an MTS controller that could apply the load either by load-or-stroke control. For this fatigue study, the load control was selected at 1Hz frequency. This load was applied to the top surface of the deck slab with a transversely centred rectangular load patch measuring 570 mm x 225 mm, having a minimum thickness of 50 mm, above a 10 mm thick rubber pad. The load patch simulated the dual tire footprint of a heavy highway vehicle. The loads were applied centrally to the deck slab between the longitudinal girders. The test set up can be seen in figures 7.7 and 7.8.

The steel loading frame consisted of a horizontal beams W 920 X 387, end supported by four vertical W 310 X 86 steel sections. The beam-to-column connections were bolted double angle web connections, designed to transfer the beam shear to column. The columns rested on concrete pedestals, which were connected through the laboratory strong floor using four anchor bolts. The use of concrete pedestals was only for the purpose of increasing the height of the loading frame to fit in the actuator and the load patch.

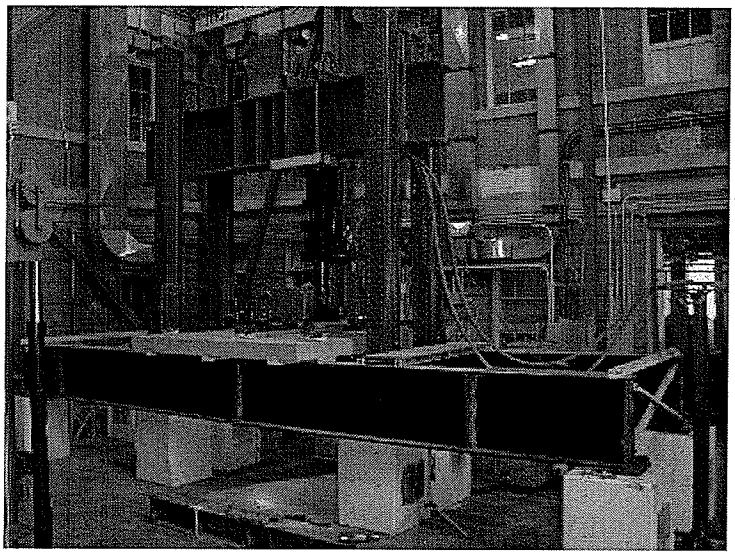

Figure 7.7
Test Set-up

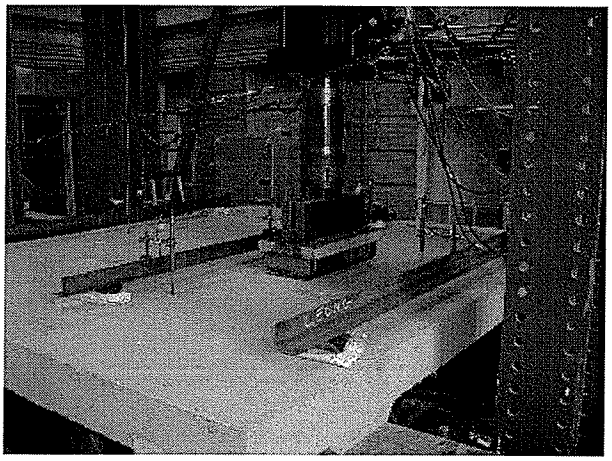

Figure 7.8
Cyclic Loading

Two ultimate load tests were also performed at the end of the fatigue study, first at the location of the cyclic testing and then at the centre of the central strap. This was done to investigate the residual strength of the deck slab.

7.3.2. Description of Instrumentation

To investigate the performance under cyclic loading, the deck slab was monitored through a number of sensors, which included linear variable displacement transducers (LVDTs), strain gauges and PI-gauges. Vertical deflection of the deck

slab was measured by LVDTs, which could measure the deflection to an accuracy of 0.01 mm In order to measure the deflection of the deck slab with respect to the girders; the LVDT's were attached to steel angles resting directly above the centre of the girders, as shown in figure 7.9. The displacement transducers were located at mid-span of the straps in the transverse direction as shown in figure 7.10, which helped us in monitoring the longitudinal and transverse profiles of deflection with respect to the number of cycles.

As mentioned previously, strain gauges were mounted along the length of the pretensioned bars to monitor the strain profile in the transverse direction and also to verify the assumption of axial stress in the strap. The position of the strain gauges in the prestressed concrete straps is shown in figure 7.10, where, C, J, and D stand for central, jacking and dead end locations respectively. The jacking and dead end strain gauges are placed 500 mm from the centre of the strap. The ultimate goal is to

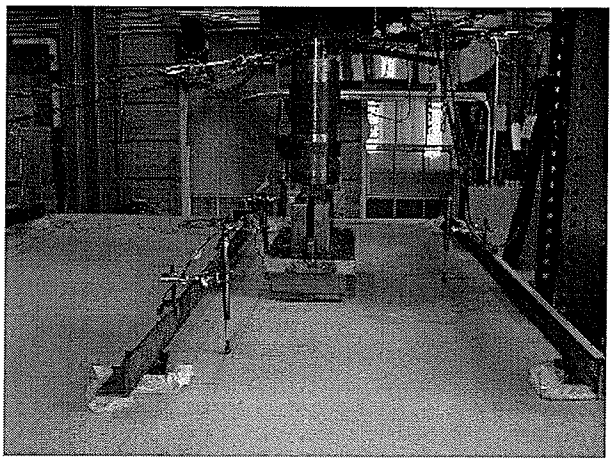

Figure 7.9
Instrumentation

monitor the cracking of the prestressed concrete strap. PI-gauge instruments were used to measure the crack width. The developing crack pattern was also recorded as the magnitude of the number of cycles increased. A typical pattern of cracking is presented and discussed later.

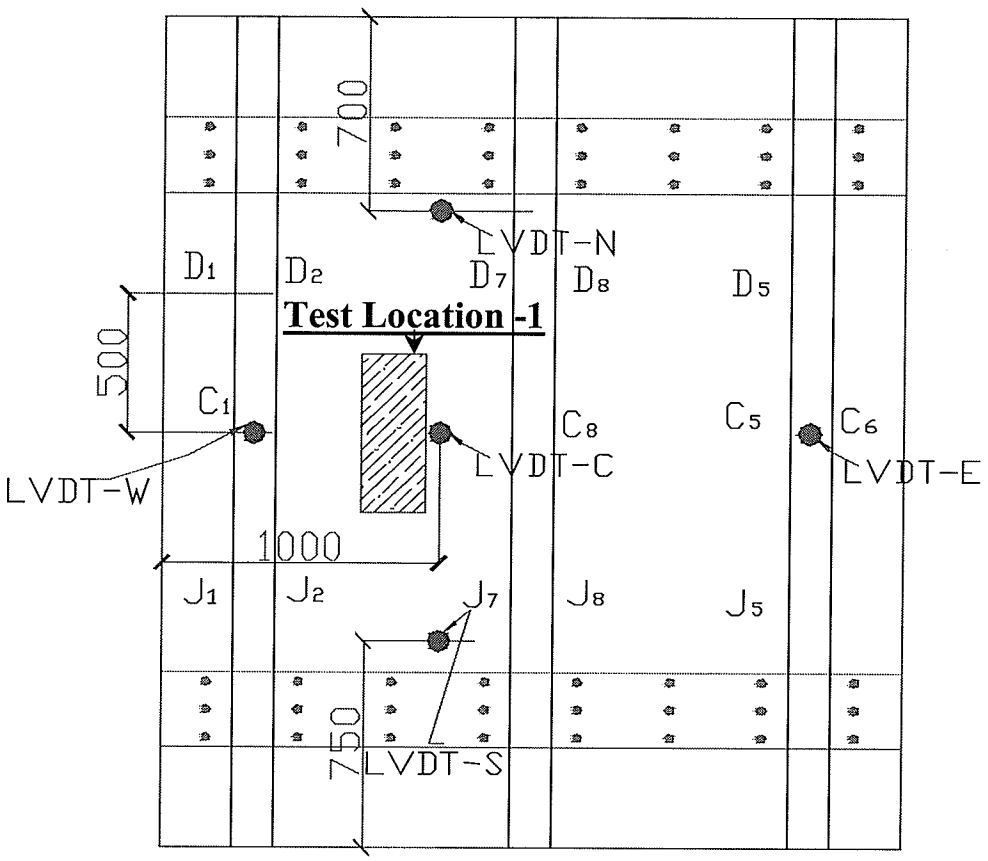

Figure 7.10
Instrumentation

7.3.3. Experimental Procedure

Initially, a load of 150 kN was applied at test location 1, which was increased in increments of approximately 10 kN. Constant pressure was maintained at each load step and the load was increased uniformly between these steps to simulate a static load with increasing magnitude. The load was increased until the 150 kN load level was reached. Then, the deck slab was subjected to a pulsating load peaking at 150 kN. After completing 9000 cycles, the load was increased to 208 kN and subjected to 500000 cycles.

On completion of the fatigue study, monotonically increasing static load was applied to determine the behaviour of the system up to failure at location 1. During this static test, the strap on the western side failed. It was decided to do one more

static test close to this location, i.e., at the centre of the central strap to gauge the reserve capacity of the system. The ability of the system to sustain significant loads in this highly deteriorated condition clearly demonstrated the validity of this design approach.

Chapter 8

EXPERIMENTAL RESULTS AND DISCUSSION

8.1. Material Tests Performed on Concrete

The compressive strength of plain concrete mix as well as of fibre reinforced concrete (FRC) was determined from cylinder tests made in accordance with ASTM C 39, making and curing concrete compression and splitting tensile strength specimens as per ASTM C 192. Compressive strength of plain concrete, before the addition of the polypropylene fibres and the superplasticizer was also measured for comparison. The results of these compressive tests as well as for the splitting tensile strengths are reported in Table 8.1.

Table 8.1: Mechanical Properties of Concrete

FRC

Physical Property	Days	Mean Strength	Modulus of Elasticity
Compressive Strength	14	51.45 MPa	-
	28	63.08 MPa	33660.5 MPa
Splitting Tensile Strength	96	4.61 MPa	

Plain Concrete

Physical Property	Days	Mean Strength	Modulus of Elasticity
Compressive Strength	28	56.96 MPa	32839.5 MPa
Splitting Tensile Strength	96	4.3 MPa	

The mean 28-day compressive strengths were calculated to be 63.08 MPa and 56.96 MPa, for the fibre reinforced and plain concrete respectively. There was a gain in strength in the concrete both in the compression as well as in splitting due to the addition of the fibres.

In accordance with section 8 of CHBDC (2000), the specified strength of concrete, f_c', should be a minimum of 30 MPa. The concrete compressive strength has only a marginal effect on the ultimate load capacity of the system. Although, the use of higher strengths concrete does not adversely affect the system (Newhook, 1997). It is worthy of mention that the high quality of deck concrete that is typically specified is needed to achieve durability and usually results in much higher strength concrete than is needed for the structural capacity of the deck.

8.2. Monitoring the Behaviour during Load Tests

The load/response history during the experiment was monitored, while applying the concentrated pulsating loads as well as the incrementally increasing static load to the concrete deck slab and measuring the strains and vertical deflections at each load cycle and at each load step.

Strains in the prestressed concrete straps were measured using electrical resistance strain gauges mounted on the GFRP bars. Using the appropriate mathematical expressions, the strains were converted to axial force in each strap. Vertical deflections of the slab were measured throughout the experiment using LVDTs.

8.3. Observed Cracking Behaviour during Testing

During the first static test followed by the dynamic tests at two load levels and the subsequent failure testing, the deck slab exhibited a characteristic sequence and pattern of cracking. This sequence can be described by the following progression of cracking:

- A relatively low magnitude of concentrated load caused a longitudinal crack on the underside of the slab, suggesting initial bending in the slab

- As the magnitude of the applied load was increased, formation of radial cracks took place which grew outward from the centre of the point of load application
- The initial cycles of the 208 kN load level cracked the strap at the centre, which was close to the free edge
- As the number of cycles increased the width of this crack increased.
- After 16000 cycles, the central crack extended throughout the length of the deck slab
- After about 100000 cycles at the 208 kN load level, the crack width increase was not very rapid.
- On the top surface, for the first static test, circumferential cracks were formed at a diameter roughly equivalent to the spacing of the girders as shown in figure 8.1.
- The radial cracks began to propagate through the slab towards its top surface as the magnitude of the applied load was increased.
- Before the shear crack could form the boundaries of the punch cone, the strap on the west side failed, resulting in the deck slab not failing in punching.

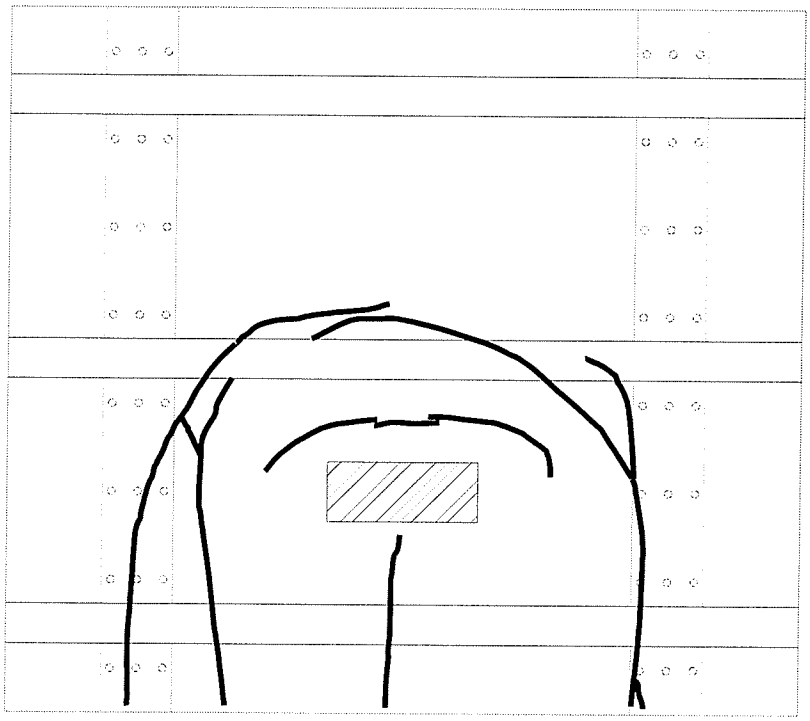

Figure 8.1
Crack Pattern – Top of the Deck Slab

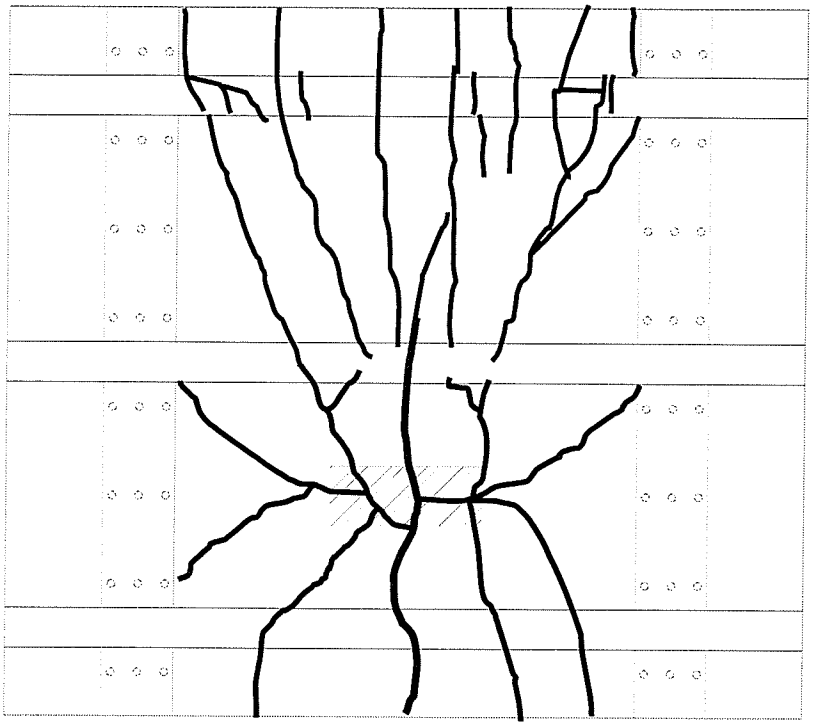

Figure 8.2
Crack Pattern – Underside of the Deck Slab

8.4. Deflection Results

The measured load-deformation curves for the first static test to 150 kN are shown in figure 8.3. The graph shows an initial linear portion, followed by a softening trend. The initial linear portion represents the system's flexural response, prior to first concrete cracking and the subsequent non-linear portion represents the slab-arching behaviour. As cracking progresses, the series of rigid bodies develop around the load and the cracked slab responds as an arch to increased loads.

It can be seen in figure 8.3, that the west deflection (LVDT W) is almost equal to the central deflection (LVDT C) and it is substantially higher than the deflection on the east side (LVDT E). It can be appreciated from figure 7.10 that a load placed midway between an inner and outer strap will induce larger load effects in the outer strap.

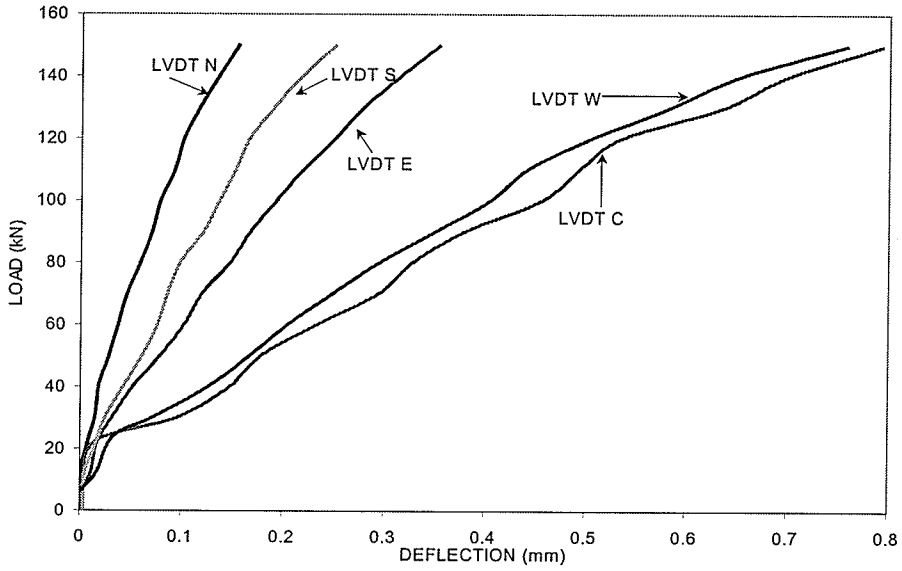

Figure 8.3
First Static Test of 150 kN

Subsequent to this static test, the deck slab was subjected to a cyclic load of 150 kN; the deflections for this test are plotted in figure 8.4 against number of cycles. The deck slab was subjected to about 9000 cycles and observing no visual damage to the system, it was decided to increase the load level to 208 kN.

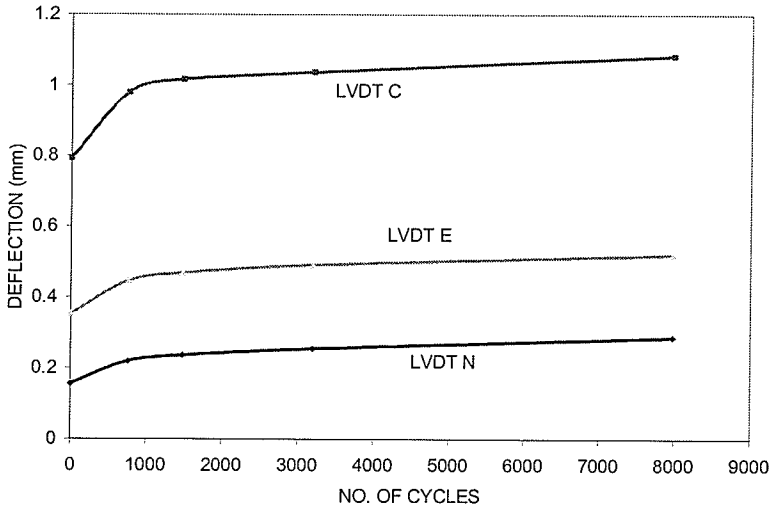

Figure 8.4
Cyclic Loading – 150 kN

There was a sharp increase in the deflections till about 30,000 cycles as can be seen in figure 8.5, suggesting progression of cracking. After 100,000 cycles, the slab seemed to stabilise. The deflections of the western strap indicated that this strap was

attracting larger axial force. The machine stroke change with the number of cycles plotted in figure 8.6 shows that even after the cracking of the western strap, there was not a sudden failure of the system. The other two straps apparently took the load and the stroke increase after 500,000 cycles was 28 percent.

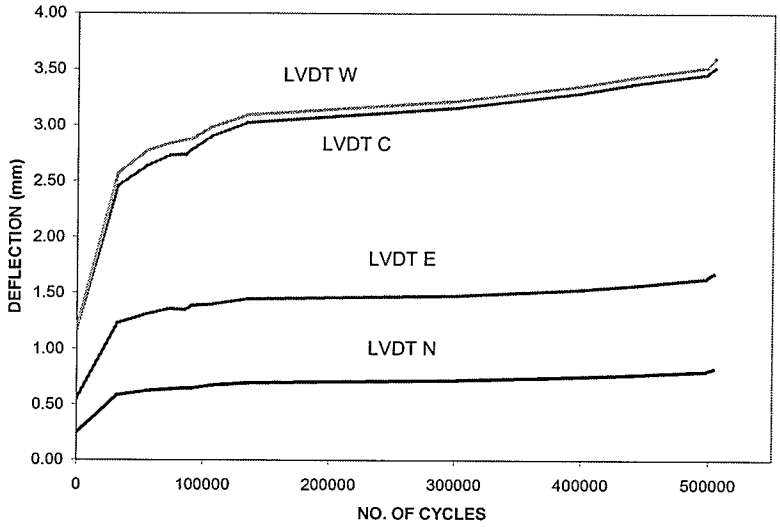

Figure 8.5
Cyclic Loading – 208 kN

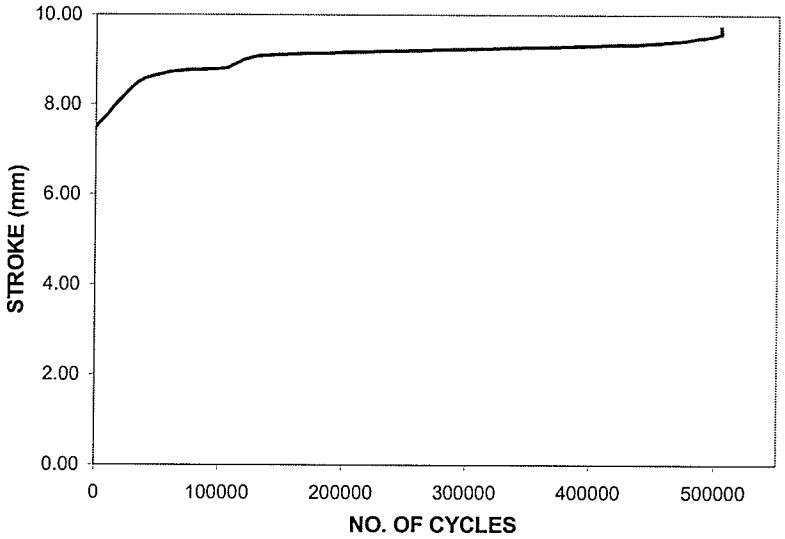

Figure 8.6
Machine Stroke – Cyclic Load of 208 kN

After the completion of 500,000 cycles, the deck slab was subjected to a failure test at the same location. The load - deflection curves for this test are shown in figure 8.7. The slope of the curve was essentially linear until a load of about 250 kN and then the

system demonstrated its highly ductile behaviour. When the load reached 350 kN, the western strap developed cracks all along its length and concrete from the strap started to spall off. At 384 kN, the strap failed with the big chunk of concrete falling off the strap, with the deflection reaching 25mm. The test was still continued with constant noises of the rupture of the GFRP fibres. When the test was finally stopped, the load had dropped to 246 kN with a deflection of about 32mm at the centre.

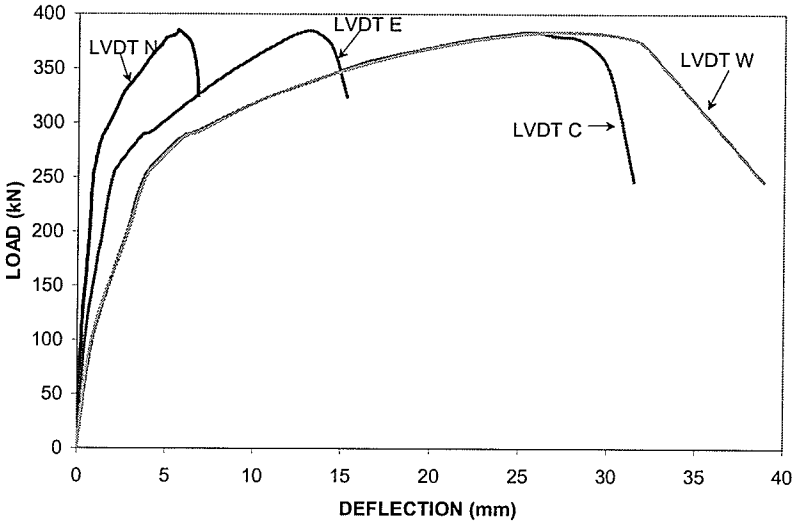

Figure 8.7
First Static Test

It was decided to do one more static test, this time at the centre of the central strap to gauge the post failure characteristics of the deck slab. The load-deflection curves for this test is shown in figure 8.8. The slope of the curves moved into the non-linear range very early in their loading histories, with the load reaching a maximum of 267 kN. Similar to the previous test, the testing was continued beyond this failure load of the central strap, but the deck slab refused to fail and it was decided to stop the test at a load of 189 kN and a central deflection of 44mm.

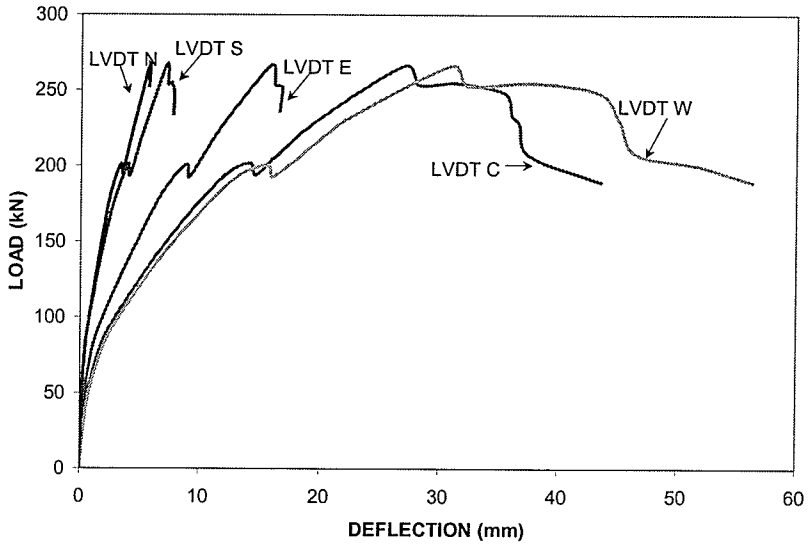

Figure 8.8
Second Static Test

8.5. Strain Results

Strap strains were measured for each test, at the rate of 16 data points/second for the cyclic test and 2-4 data points/ second for the static test.

For the first static test, the load - strain curves are shown in figure 8.9 for all the three straps. The strains at the centre of the straps on each side of the load patch were very high as compared to those at the ends, whereas the strains in the eastern strap were nearly uniform along its length. Figure 8.9 shows that, although, the load was applied centrally between the western strap and the central strap, the end strap resisted a greater load.

Figure 8.10 shows the strap strain plotted against the number of cycles for a pulsating load of 150 kN. The strain at the centre of the western strap reached a level very close to the cracking strain, which was determined from the axial tensile tests on the prestressed concrete straps as about 400 microstrain. After 1000 cycles, the strain increase was not very dramatic and was reaching a level of stabilisation.

After only a couple of cycles at the 208 kN load level, the western strap cracked which is showed by the increase in strain in figure 8.11. Because of the cracking of the

west strap, some load was transferred to the other two straps, which is shown by their corresponding increase in strains. As mentioned previously, similar to the deflection results, the strain increase after 100,000 cycles was not very sudden.

For the first static test, the load-strain responses for all the straps were very similar to those observed in the axial tests done on the straps (figure 8.12). The cracking strain was approximately 400 microstrain. For a wheel load of about 350 kN, the strain in the strap corresponds an axial force of 220 kN in the strap, which is much higher than in a typical steel strap, suggesting higher stiffness of the strap attracts higher force.

By the end of the first static test, the western strap was totally damaged and the other straps also had developed large cracks. Consequently, the load-strain curves were very different for the second static test than the previous test. As the load was increased, gradually, the central strap failed, transferring the load to the eastern strap as suggested by the strain profile of the eastern strap, presented in figure 8.13.

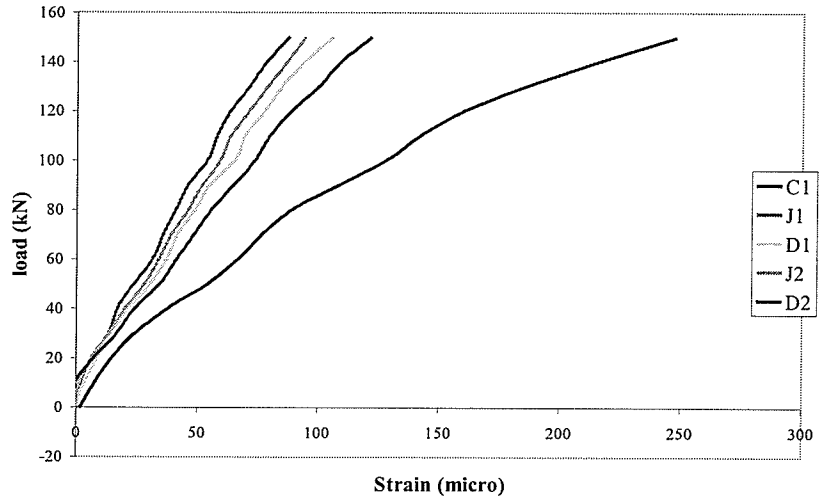

West Strap

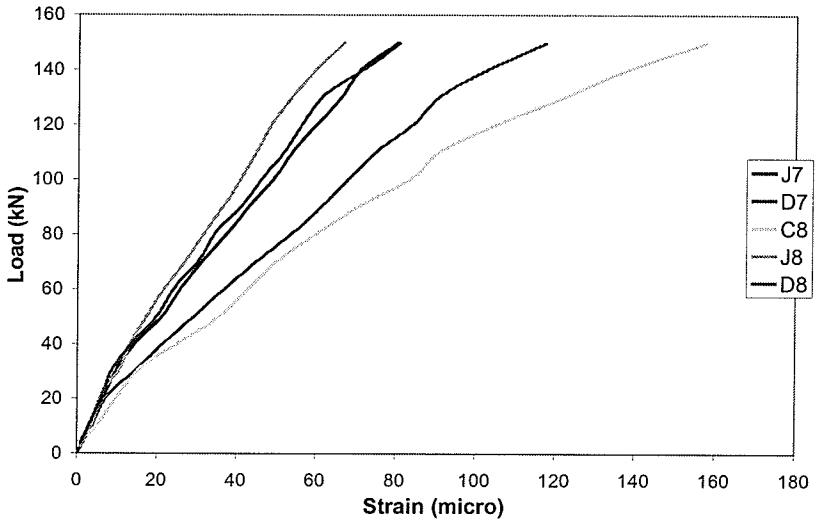

Centre Strap

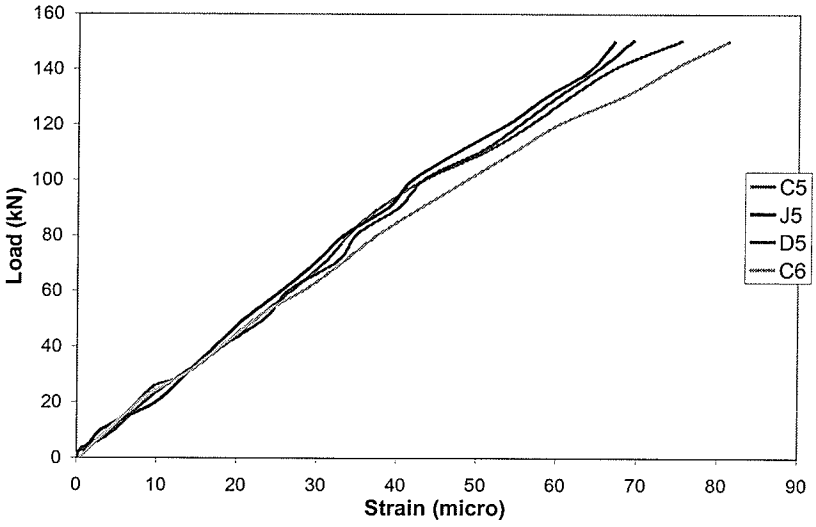

East Strap

Figure 8.9
Strains in Strap-First static Test – 150 kN

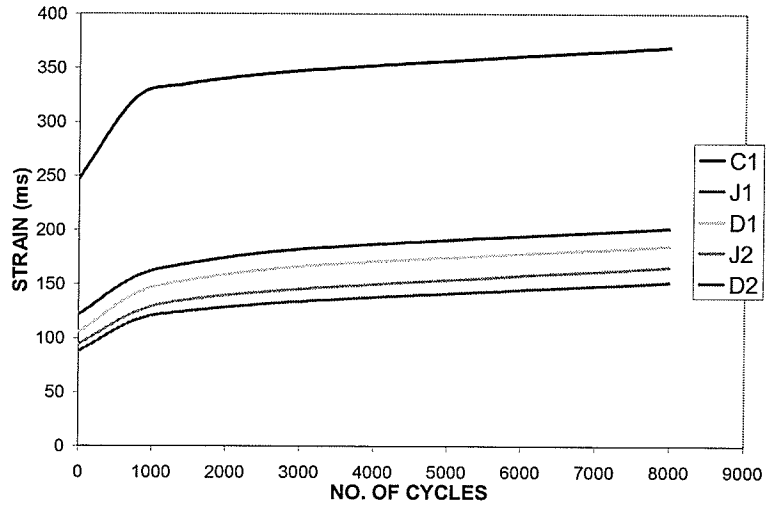

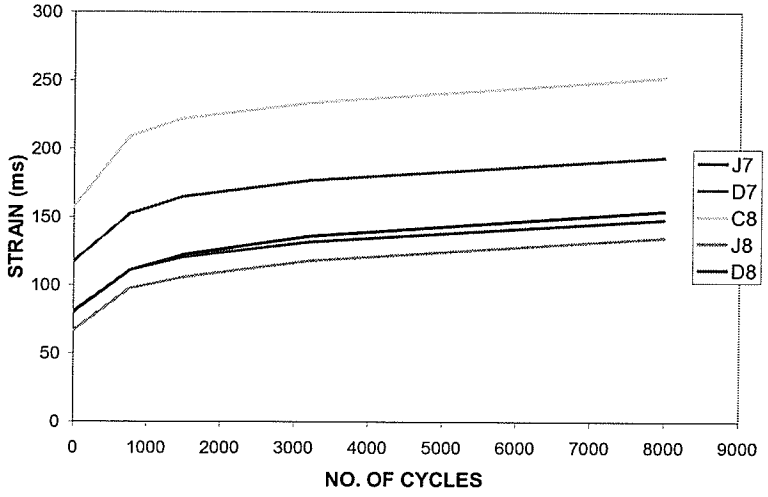

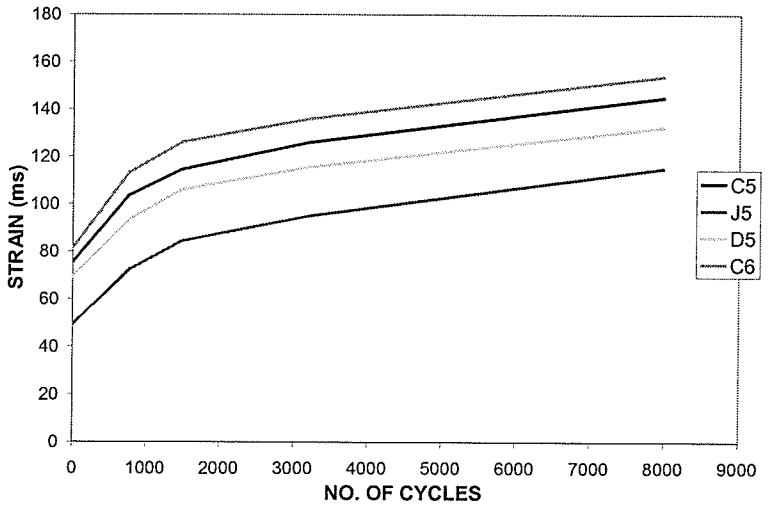

Figure 8.10
Strains in Straps - Cyclic Test – 150 kN

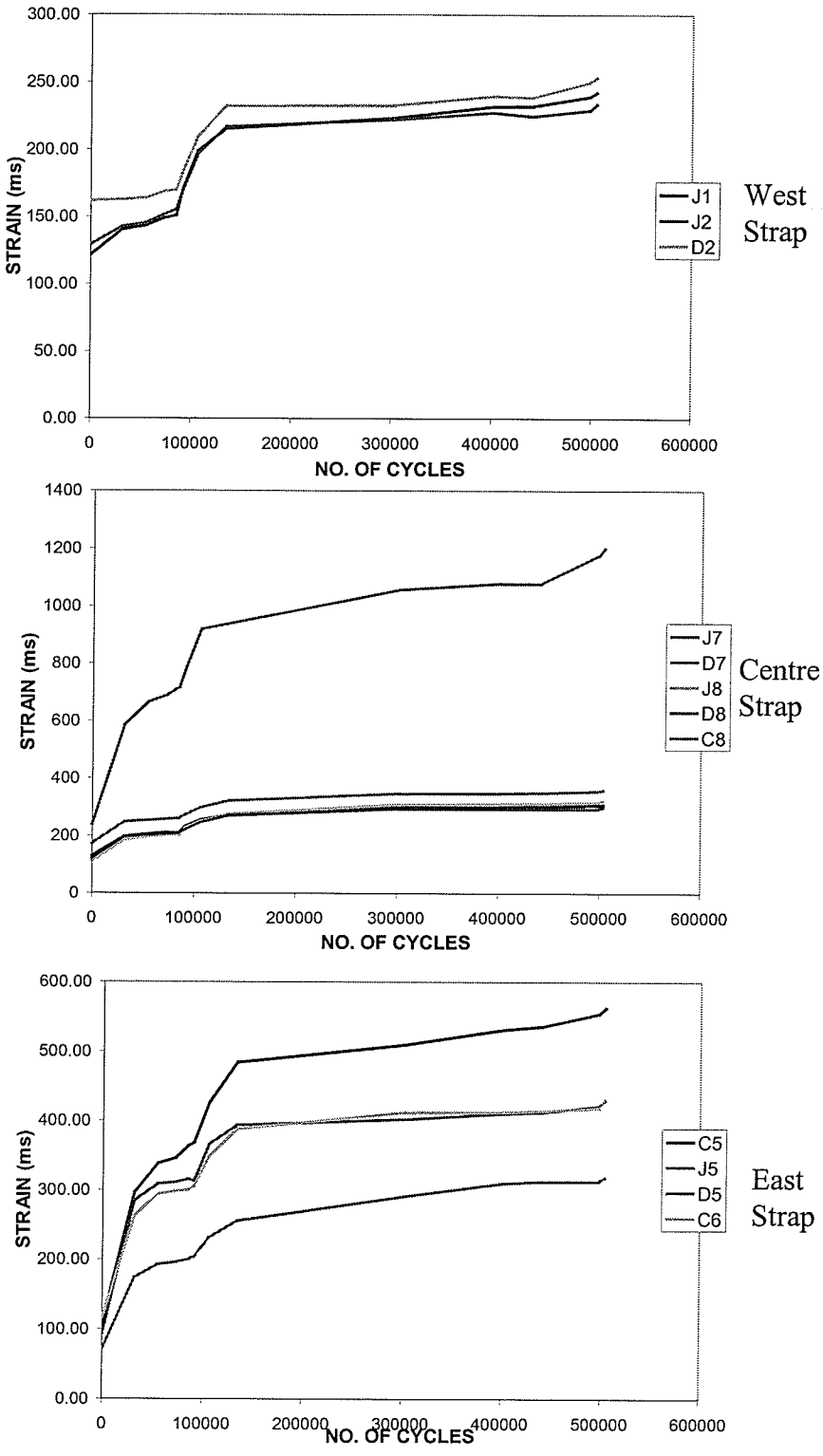

Figure 8.11
Strains in Strap - Cyclic Test – 208 kN

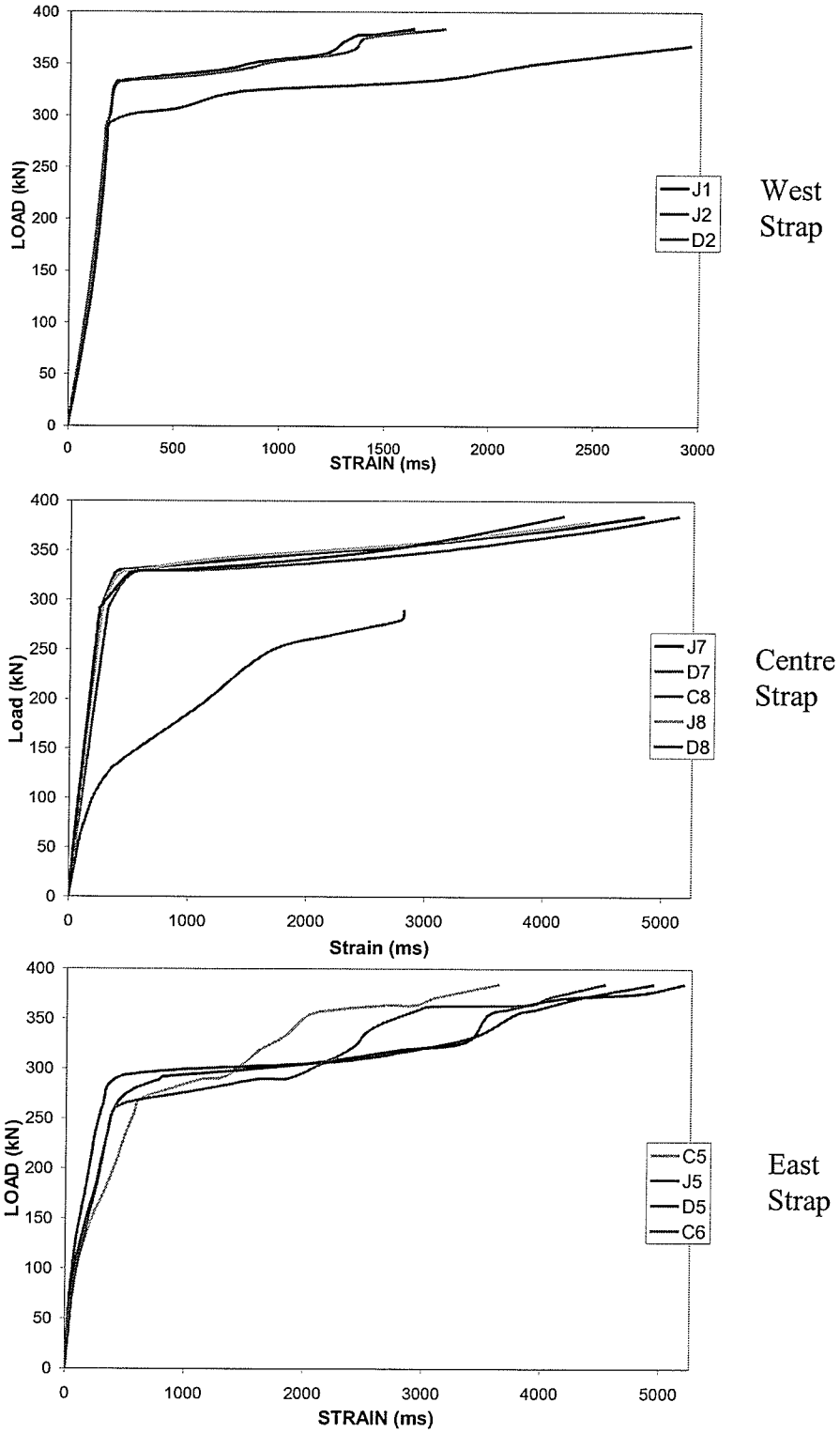

Figure 8.12
Strains in Strap - First Static Test

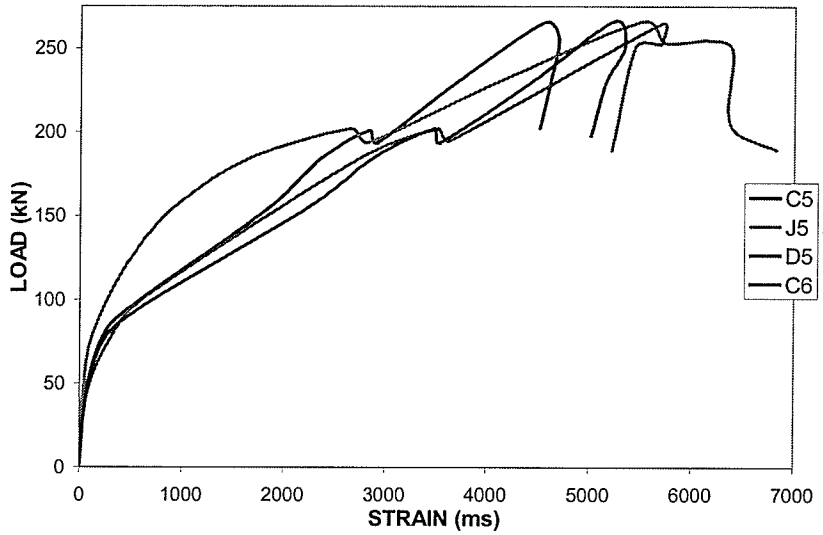
250
200
150
100
50
0
LOAD (kN)
0
1000
2000
3000
4000
5000
6000
7000
STRAIN (ms)
C5
J5
D5
C6

Chapter 9

CONCLUSIONS AND RESEARCH NEEDS

The study has shown that prestressed concrete straps can be used to confine steel free deck slab laterally. Although the static failure load of a deck slab with Prestressed concrete strap is significantly lower the conventional steel free deck slab or reinforced concrete deck slab, having sustained half million cycles of maximum lifetime wheel load (i.e. 207 kN) suggests that its fatigue resistance is as good as other deck slabs considered.

The following conclusions emerged from the research study reported in this thesis.

- Due to the low cracking capacity and stiffness, RC straps are not recommended for lateral confinement of steel free deck slabs
- The grips used for testing the GFRP bar in axial tension developed full strength without failure of the bar in the anchorage zone. The GFRP bars failed in the gauge length portion of the bar, as required by S806-02.
- The couplers devised for stressing the GFRP tendon and keeping it in a stressed position worked well without slip during prestressing process.
- Uncracked prestressed concrete straps with GFRP tendons have more than twice the stiffness of conventionally used steel straps 50 x 25 mm in cross-section.
- Having sustained half a million cycles of the maximum lifetime wheel load, the fatigue resistance of the proposed concept is as good as the conventionally used steel free deck slabs with steel straps as lateral confinement.
- The static failure load of the deck slab with prestressed concrete strap as transverse confinement was 384 kN and the deck slab demonstrated substantial amount of ductility. The extent of ductility was evident in the second static test, when the deck slab refused to fail and the test had to be terminated.
- The use of PC straps is feasible for the lateral confinement of steel free deck slabs.

The following recommendations can be incorporated in the further/future studies involving FRP tendons and transverse confinement for steel free deck slabs:

- Use of aramid fibre tendons instead of GFRP tendons as they have 75 % higher strength, almost similar elastic modulus as that of concrete and excellent fatigue characteristics
- The issue of durability of glass fibres in alkali environment is still a big concern and should be used with alkali resistant concrete. Work is currently being carried out at the University of Manitoba, which deals with exposing pretensioned GFRP bars to an alkali environment and observing them under a SEM (Scanning Electron Microscope) for degradation of the fibre/matrix interface. An axial load test carried out by the author on GFRP tendons extracted from previously tested year old prestressed concrete strap showed that the strength reduction was about 13%. This could be attributed to the initial damage due to prestressing.
- A fatigue analysis of the connection between the transverse prestressed concrete strap and the deck slab as well as dynamic loading of prestressed concrete strap should be explored quantitatively
- Testing of deck slab under sequential or moving wheel load should be carried out to correctly simulate the effect of a vehicle
- Further improvement in the instrumentation are recommended to better understand the behaviour of steel free deck slab with prestressed concrete strap as transverse confinement –
    - Measurement of the lateral displacement of the girders
    - Measurement of strains in the cross bracing

Chapter 10

REFERENCES

1. ASTM C 39/C 39M-99. "Standard Test Method for Compressive Strength of Cylindrical Concrete Specimens". ASTM, 100 Barr Harbor Drive, West Conshohocken, PA 19428.

2. ASTM C 143/C 143M-98. "Standard Test Method for Slump of Hydraulic Cement Concrete". ASTM, 100 Barr Harbor Drive, West Conshohocken, PA 19428.

3. ASTM C 469-94. "Standard Test Method for Static Modulus of Elasticity and Poisson's Ratio of Concrete in Compression". ASTM, 100 Barr Harbor Drive, West Conshohocken, PA 19428.

4. ASTM C 496-96. "Standard Test Method for Splitting Tensile Strength of Cylindrical Concrete Specimens". ASTM, 100 Barr Harbor Drive, West Conshohocken, PA 19428.

5. ASTM C 995-94. "Standard Test Method for Time of Flow of Fiber-Reinforced Concrete Through Inverted Slump Cone". ASTM, 100 Barr Harbor Drive, West Conshohocken, PA 19428.

6. Aly, A., Bakht, B., Schaefer, J. 1997. Design and Construction of a steel-free deck slab in Ontario. Proceedings, Annual Conference - Canadian Society for Civil Engineering, v 6, 1997, Structures - Composite Materials, Structural Systems, Telecommunication Towers, Proceedings of the 1997 Annual Conference of the Canadian Society for Civil Engineering. Part 6 (of 7), Sherbrooke, Can, pp. 81-90.

7. Bakht, B., Mufti A.A., Tadros, G., 2000. "Failure test on unreinforced concrete slab on stay-in-place metal forms". Technical Report, ISIS Canada, University of Manitoba.

8. Bakht, B., Agarwal, A.C., 1993. "Deck Slabs of Skew Girder Bridges". Proceedings, CSCE Annual Conference held in Fredericton, pp. 55-56. 1993.

9. Bakht, B., Mufti A.A., 1998. "Five steel-free deck slabs in Canada". Journal of the International Association for Bridge and Structural Engineering (IABSE), 8(3), pp. 196-200.

10. Bakht, B., and Lam, C., 1997. "Behavior of transverse confining systems for Steel-free Deck Slabs". Research report. Structures Research office, Ministry of Transportation Ontario, Downsview, Ontario.

11. Bakht, B., and Aly, A., 1997. "Testing in isolation of transverse confining systems for Steel Free Deck slabs", Canadian Journal of Civil Engineering, 25(4), pp. 789-786.

12. Bakht, B., and Jaeger, L.G., 1994, "Revisiting Prestress Losses in Stress-Laminated Wood Decks", Proceedings: Annual Conference of the Canadian Society for Civil Engineering, 1994, pp. 31-40.

13. Bakht, B., Lam, C., Bolshakova, T., 1997. " The first Stressed Log Bridge – Recent advances in Bridge Engineering", Proceedings of US-Canada-Europe Workshop on Bridge Engineering, Zurich, pp. 159-166.

14. Batchelor, B. DeV., Taylor, R. J., Van Dalen, K., 1982. "Prestressed Wood Bridges". International Conference on Short and Medium Span Bridges, Proceedings, v 2, Toronto, Ontario, Can, pp. 203-218.

15. Beal, D.B., 1982. "Load Capacity of Concrete Bridge Decks". ASCE Journal of the Structural Division, 108 (ST4): 814-832.

16. Benmokrane, B., Chekired, M., and Nicole, J. F., 1998. Evaluation of the Joffre concrete bridge decks reinforced with FRP rebars and grids: Progress Technical Report submitted to the Ministry of Transportation of Quebec, 50 pages.

17. Benmokrane, B., and Masmoudi, R., 1996. "FRP C-Bar as reinforcing rod for concrete structures". Proceedings - 2nd International Conference on Advanced Composite Materials in Bridges and Structures, Montreal, pp. 181-188.

18. Black, C.J., Tsai, P.C., and Ventura, C.E., 1997. Ambient vibration measurements of the University Drive/ Crowchild Trail Bridge in Calgary, Alberta. The University of British Columbia Earthquake engineering Research Report EQ 97-005. Technical Report prepared for ISIS Canada.

19. CHBDC, 2000. "Canadian Highway Bridge Design Code". CAN/CSA-S6-00, 178 Rexdale Boulevard, Toronto, Ontario, Canada M9W 1R3.

20. Commentary on CHBDC, 2000. "Calibration Report". Commentary on CAN/CSA-S6-00, Canadian Highway Bridge Design Code S6.1-00, 178 Rexdale Boulevard, Toronto, Ontario, Canada M9W 1R3.

21. Carreira, Domingo J., and Chu, Kuang-Han., 1986. "Stress-Strain Relationship for Reinforced Concrete in Tension". Journal of the American Concrete Institute, v 83, n 1, pp. 21-28.

22. CSA – S806-02, 2002. "Design and Construction of Building Components with Fibre-Reinforced Polymer". Canadian Standard Association, 178 Rexdale Boulevard, Toronto, Ontario, Canada M9W 1R3.

23. CSA A23.3-94, 1995. "Design of Concrete Structures". Canadian Standard Association, 178 Rexdale Boulevard, Toronto, Ontario, Canada M9W 1R3.

24. Collins, M.P. and Mitchell, D., 1997. Prestressed Concrete Structures, Response Publications, Canada.

25. Erki, M.A., Rizkalla, S.H., 1993. "Anchorages for FRP". Concrete International: Design and Construction, v 15, n 6, pp. 54-59.

26. Fang, I.K., Worley, J.A., Burns, N.H., and Klinger, R.E., 1986. "Behavior of Ontario type bridge decks on Steel girders". Research Report 350-1, Center for Transportation Research, The University of Texas at Austin.

27. Guide for the Design and Construction of Concrete Reinforced with FRP Bars, Reported by ACI Committee 440, American Concrete Institute, P.O. Box 9094, Farmington Hills, Michigan 48333-9094.

28. Hewitt, B.E., and Batchelor, B., 1975. "Punching shear strength of restrained slabs". ASCE, Journal of the Structural Division, 101(STP9): 1837-1853.

29. Jackson, P.A., and Cope, R.J., 1990. "The behavior of deck slabs under full Global loads". Developments in Short and Medium Span Bridge Engineering '90, Vol.1, pp. 253-264. Canadian Society for Civil Engineering.

30. Jaeger, L. G., Bakht, B., 1993. "Reliability of concrete strength prediction from limited test data". Canadian Journal of Civil Engineering, v 20, n 6, pp. 980-987.

31. JSCE, 1997. "Recommendation for Design and Construction of Concrete Structures using Continuous Fiber Reinforcing Materials". Research Committee on Continuous Fiber Reinforcing Materials, Japan Society of Civil Engineers, Yotsuya 1-chome, Shinjyuku-ku, Tokyo, 160 Japan.

32. Keesler, R.J., and Powers, R.G., 1988. "Corrosion of Epoxy Coated Rebars – Keys Segmental Bridge – Monroe County". Report No. 88-8A, Florida Dept. of Transportation, Materials Office, Corrosion Research Laboratories, Gainesville, Fla.

33. Kommandigesellschaft, D., and Kommandigesellschaft, W., 1963. "Concrete Pavement with Prestressed Concrete Bars as Reinforcement," PCA Foreign Literature study No. 442, Munich, 19 pp. (in German).

34. Matsui, S., Tokai, D., Higashiyama, H., and Mizukoshi, M., 2001. "Fatigue Durability of Fiber Reinforced Concrete Decks under Running Wheel Load". Proceedings of the Third International Conference on Concrete under Severe Conditions, CONSEC' 01, Vancouver, British Columbia, Volume 1, pp. 982-991.

35. Mufti, A.A., Memon, A.H., Bakht, B., and Banthia, N., 2002. "Fatigue Investigation of Steel-Free Bridge Deck Slabs". ACI International SP – 206, pp. 61-70.

36. Mufti, A.A., Bakht, B., Jaeger, L.G., 1991. "FRC Deck Slabs with Diminished Steel Reinforcement". Proceedings, IABSE Symposium held in Leningrad, pp. 388-389.

37. Mufti, A.A, Jaeger, L.G., Bakht, B., Wegner, L.D., 1993. Experimental investigation of FRC deck slabs without internal reinforcement. Canadian Journal of Civil Engineering, 20(3), pp. 398-406.

38. Mufti, A.A, Newhook, J.P., 1998. "PUNCH Program" User Manual, Dalhousie University.

39. Newhook, J.P., Mufti, A.A., 1996. "A Reinforcing Steel-Free Concrete Deck Slab for the Salmon River Bridge". Concrete International, Vol.18, No.6.

40. Newhook, J.P., 1997. "The Behavior of Steel-Free Concrete Bridge Deck Slabs under Static Loading Conditions". Ph.D. Thesis, Dalhousie University, Halifax, Nova Scotia.

41. OHBDC, 1979. "Ontario Highway Bridge Design Code". 1st Edition, Highway Engineering Division, Ministry of Transportation, Downsview, Ontario, Canada.

42. Perdikaris, P.C. Beim, S., 1988. "RC Bridge Decks under Pulsating and Moving Loads". ASCE Journal of Structural Engineering. 114 (3), pp. 591-607.

43. Rizkalla, S., Shehata, E., Abdelrahman, A., Tadros, G., 1998. "New generation". Concrete International, v 20, n 6, pp. 35-38: American Concrete Institute, Farmington Hills, MI, USA.

44. Svecova, D., Razaqpur, A.G., 2000. "Flexural behavior of concrete beams reinforced with carbon fiber-reinforced polymer prestressed prisms". ACI Structural Journal, V.97, N. 5.

45. Thorburn, J., 1996, "A Study of Externally Reinforced Fibre-Reinforced Concrete Bridge Decks on Steel Girders". Ph.D. Thesis, Dalhousie University, Halifax, Nova Scotia.

46. Thorburn, J., and Mufti A.A. 1995., "Full-scale testing of externally reinforced FRC bridge decks on steel girders". Proceedings, Annual Conference of CSCE held in Ottawa, V.II, pp. 543-552.

47. Vogel, H., 2002. "Durability and Thermal Compatibility of FRP in Concrete". Project Report Presented to the Department of Civil Engineering, Faculty of Engineering, The University of Manitoba.